Oceanologia, uncorrected, in press
Polish Academy of Sciences
Institute of Oceanology

https://doi.org/10.5697/PKCT9576

Spatial and temporal variability of aerosol optical depth over the Baltic Sea based on MERRA-2 and CAMSRA reanalyses

Anna Rozwadowska*, Piotr Markuszewski

Abstract
The spatial and temporal variability of aerosol optical depth (AOD) over the Baltic Sea was analysed using two atmospheric reanalyses: MERRA-2 (1980–2023) and CAMSRA (2003–2023). The study examined total and speciated AOD at 550 nm – sulphate, organic, black carbon, sea salt, and dust – focusing on spatial patterns, long-term trends, seasonal cycles, and relationships with fire activity and the North Atlantic Oscillation (NAO). Both reanalyses show a south-to-north decrease in total AOD, with basin-mean values of 0.221 (1980–1999, MERRA-2), 0.135 (2003–2023, MERRA-2), and 0.116 (2003–2023, CAMSRA). The long-term trends are negative (-0.073 [62% confidence intervals: -0.111; -0.045] per decade, significant at a 90% confidence level, -0.006 [-0.009; -0.002] per decade, insignificant, and -0.016 [-0.021; -0.009] per decade, significant at a 90% confidence level, respectively), being strongest over the southern Baltic Sea and weaker in the north. The seasonal AOD cycle changed from a single spring maximum in the late 20th century to a dominant summer maximum after 2012. Fire activity shows its strongest correlation with total and black carbon AOD in spring, while the NAO index correlates positively with sea-salt AOD in winter and negatively in July. The greatest agreement between AOD characteristics derived from MERRA-2 and CAMSRA was found for total AOD and sea salt AOD.

Keywords
Aerosol optical thickness; Aerosol optical depth; Baltic Sea; MERRA-2; CAMSRA; Trend; Seasonal cycle; Spatial variability; NAO index; Fires

Institute of Oceanology, Polish Academy of Sciences, Powstańców Warszawy 55, 81–712 Sopot, Poland
***Correspondence**: ania@iopan.pl (A. Rozwadowska)

Received: 3 November 2025; **revised:** 4 March 2026; **accepted**: 28 April 2026

Abbreviations

- AATSR/Envisat – Advanced Along-Track Scanning Radiometer (explained)
- ACCMIP – Atmospheric Chemistry and Climate – Model Intercomparison Project (Appendix)
- ADAS – Atmospheric Data Assimilation System (explained)
- AeroCom – AEROsol COMparisons between Observations and Models
- AERONET – AErosol RObotic NETwork
- AOD – aerosol optical depth; in sections 4 and 5 AOD(550)
- AOD(550) – aerosol optical depth at a wavelength of 550 nm
- AOD_BC – AOD for black carbon at a wavelength of 550 nm
- AOD_DU – AOD for dust at a wavelength of 550 nm
- AOD_OC – AOD for organic aerosol (organic carbon; in MERRA-2) at a wavelength of 550 nm
- AOD_OM – AOD for organic aerosol (organic matter; in CAMSRA) at a wavelength of 550 nm
- AOD_SS – AOD for sea salt aerosol at a wavelength of 550 nm
- AOD_SU – AOD for sulphate aerosol at a wavelength of 550 nm
- AVHRR – Advanced Very High Resolution Radiometer

- CAMS – Copernicus Atmosphere Monitoring Service
- CAMSRA – CAMS Reanalysis
- DMS – dimethyl sulphide
- EDGAR – Emissions Database for Global Atmospheric Research
- ESDIS – NASA's Earth Science Data and Information System (explained)
- FIRMS – Fire Information for Resource Management System
- GEOS-5 – Goddard Earth Observing System Model, Version
- GFASv1.2 – Global Fire Assimilation System, version 1.2 (Appendix)
- GFEDv3.1 – Global Fire Emission Dataset, version 1.2 (Appendix)
- GOCART – Goddard Chemistry, Aerosol, Radiation, and Transport model
- IFS – Integrated Forecast System
- JRAero – Japanese Reanalysis for Aerosol (explained)
- MEGAN model – Model of Emissions of Gases and Aerosols from Nature (Appendix)
- MERRA-2 Modern-Era Retrospective Analysis for Research and Applications, Version 2 Reanalysis
- MISR – Multi-angle Imaging Spectroradiometer (explained)
- MODIS – Moderate Resolution Imaging Spectroradiometer
- NAAPS-RA – Navy Aerosol Analysis and Prediction System reanalysis
- NAO – North Atlantic Oscillation
- NASA – National Aeronautics and Space Agency
- NASA GES DISC – NASA Goddard Earth Sciences (GES) Data and Information Services Center (DISC)
- ns – statistically non-significant
- POM – particulate organic matter (Appendix)
- QFED – Quick Fire Emissions Dataset (Appendix)
- RCP – Representative Concentration Pathway (Appendix)
- RETRO - REanalysis of the TROpospheric chemical composition over the past 40 years (Appendix)
- RMSE – Root Mean Square Error (Appendix)
- SNAO – Summer NAO
- SPARTAN network – Surface PARTiculate mAtter Network (explained)
- ss90 – statistically significant at the 90
- ss95 – statistically significant at the 95
- VOC – volatile organic compounds (Appendix)

1. Introduction

The Baltic Sea is an inland sea located in northwestern Europe, connected to the North Sea and the Atlantic Ocean through the Danish Straits. It lies between maritime temperate and continental subarctic climate zones (Meier et al., 2022) and is influenced by relatively mild and humid marine air masses from the North Atlantic and continental air masses from Eurasia, with occasional intrusions of Arctic and subtropical air (Rutgersson et al., 2014). Despite this variability, westerly flow from the ocean predominates.

The strong variability of air masses and atmospheric conditions over the region leads to pronounced spatial and temporal changes in aerosol properties (Zdun et al., 2016). Major anthropogenic aerosol sources are located in the southern Baltic region (Mancinelli et al., 2024). Local marine sources include wind-driven emissions of sea-spray aerosol (Petelski et al., 2014; Markuszewski et al., 2017), emissions of biogenic aerosols and their precursors like dimethyl sulphide (Lewandowska et al., 2017; Thakur et al., 2022), and ship emissions (Kecorius et al., 2016; Karl et al., 2019). Modelling results show that European emissions account for over 80% of near-surface sulphate, black carbon, and organic aerosol mass in the southern Baltic and 40–60% in the northern Bay of Bothnia (Yang et al., 2020). Consequently, mean aerosol optical depth (AOD) decreases from south to north (Mancinelli et al., 2024).

The atmosphere in the Baltic region is also affected by long-range transport. Biomass burning aerosol from North America (Markowicz et al., 2016; Shang et al., 2021) and Saharan dust intrusions (Ansmann et al., 2003) are periodically observed. According to Yang et al. (2020), non-European sources contribute 69% of sulphate, 28% of black carbon, and 40% of primary organic aerosol burden over northwestern Europe.

Since the 1980s, European AOD has markedly declined due to emission reductions. Yang et al. (2020) reported a decrease in total aerosol optical depth at 550 nm (AOD(550)) from 0.12–0.13 to 0.06–0.07 between 1980 and 2018 in northwestern Europe, with 91% of this reduction attributed to European sources. MODIS-based studies (Moderate Resolution Imaging Spectroradiometer; Glanz et al., 2019; Di Antonio et al., 2023) confirmed spatially variable but mostly negative AOD trends over Europe.

Glanz et al. (2019) reported MODIS-based AOD trends over the southwestern and western Baltic Sea ranging from −0.026 to −0.017 per decade (1/10y; 2003–2017, April–September). Using MODIS Terra data (2000–2023), Han et al. (2025) found seasonal AOD trends over the Baltic Sea of −0.0084 1/10y (all data), −0.116 1/10y in spring and +0.025 1/10y in summer, which indicates significant seasonal variations.

Over land, trends vary strongly with the AOD data source (e.g., MODIS, AErosol RObotic NETwork – AERONET, reanalysis), the exact period and location. During the 21st century, the AOD(550) trend ranged from −0.026 1.10y at Toravere, Estonia (AERONET, 2002–2020) to +0.010 1/10y for Gustav Dalen, Sweden (MERRA-2, 2005–2020) (Glanz et al., 2019, 2022; Filonchyk et al., 2020; Markowicz et al., 2022). Mancinelli et al. (2024) showed consistent AOD and sulphate AOD decreases over Baltic capitals from 1989 to 2019, with localised increases in organic and black carbon components in some cities. Seasonal AOD cycles also differ widely – for example, displaying maxima in April (AERONET Gotland, 1999–2005; Zdun et al., 2011) or July (MODIS over Poland, 2000–2018; Filonchyk et al., 2020).

Most previous studies focused on land areas (Glanz et al., 2022; Markowicz et al., 2022; Mancinelli et al., 2024), selected Baltic Sea subregions (Glanz et al., 2019; Di Antonio et al., 2023), and/or warm months (Glanz et al., 2019), leaving year-round variability and open-sea conditions insufficiently characterised. AOD measurements, both from ground-based and satellite-borne instruments, are limited to cloudless days or days with little to moderate cloud cover. AOD measurements are particularly limited in winter and autumn, when typically heavy cloud cover is combined with low solar altitude and short days, especially in the northern Baltic Sea. Consequently, aerosol reanalyses provide a valuable complement, offering continuous coverage and seasonal completeness. Major global reanalyses include CAMSRA – Copernicus Atmosphere Monitoring Service Reanalysis (Inness et al., 2019), JRAero – Japanese Reanalysis for Aerosol (Yumimoto et al., 2017), MERRA-2 – Modern-Era Retrospective Analysis for Research and Applications version 2 (Randles et al., 2017), and NAAPS-RA – Navy Aerosol Analysis and Prediction System reanalysis (Lynch et al., 2016), which differ in their underlying meteorological models, aerosol species design, aerosol sources, representations of aerosol processes, as well as data assimilation methods and AOD observation processing (Xian et al., 2024). Xian et al. (2024) found that although the global distribution and magnitude of total AOD agree well across all four reanalyses, the relative differences in speciated AODs were considerably larger. Compared to other reanalyses, CAMSRA yields higher organic and lower sulphate AOD globally. In Europe, CAMSRA (Witthuhn et al., 2021), MERRA-2 (Markowicz et al., 2022, 2024; Mancinelli et al., 2024), and NAAPS (Maciszewska et al., 2010) have been most widely applied in aerosol studies.

Given (1) the large longitudinal extent of the Baltic Sea with the main anthropogenic aerosol sources in the south, (2) the lack of regular ground-based AOD measurements from the open sea, (3) the scarcity of measurements from the autumn and winter due to high cloud cover, and (4) the differences among reanalyses, the objective of this study is to characterise the spatial and temporal variability of total and speciated AOD(550) over the Baltic Sea using MERRA-2 (1980–2023) and CAMSRA (2003–2023), with particular attention to their similarities and differences. Additionally, we assess the influence of regional fires and the North Atlantic Oscillation (NAO) index on monthly AOD variations. We specifically aim to assess: (1) how AOD trends differ across sectors, aerosol species, and reanalyses, (2) how CAMSRA and MERRA-2 compare in their depiction of AOD seasonality, (3) how interannual AOD fluctuations vary in time and space, and (4) whether fire activity and NAO significantly modulate interannual AOD variability.

The outline of the paper is as follows: Section 2 briefly presents the MERRA-2 and CAMSRA reanalyses and auxiliary datasets (NAO indices and fire data); Section 3 describes the methods; Section 4 presents the results and discussion; and Section 5 summarises the findings.

2. Materials

2.1 Reanalyses

2.1.1 MERRA-2

The Modern-Era Retrospective analysis for Research and Applications, Version 2 (MERRA-2) is NASA's atmospheric reanalysis available from 1980 onward (Randles et al., 2017 and references therein). It uses the Goddard Earth Observing System Model, Version 5 (GEOS-5) coupled with the Atmospheric Data Assimilation System (ADAS), version 5.12.4.

Aerosols are simulated using the Goddard Chemistry, Aerosol, Radiation, and Transport model (GOCART; Chin et al., 2002; Colarco et al., 2010) integrated into the GEOS-5 modelling system. GOCART simulates several aerosol species and aerosol precursors: organic carbon (OC), black carbon (BC), sea salt (SS), dust (DU), and sulphate aerosols (SO4), as well as dimethyl sulphide (DMS), and sulphur dioxide (sulphate aerosol precursors). The modelling of aerosol in MERRA-2 is presented in Appendix 1 and discussed in detail in Randles et al. (2017). The resolution of the MERRA-2 data is 0.5° × 0.625° with a temporal resolution of 1 h.

MERRA-2 assimilates bias-corrected AOD(550) observations from AVHRR (over the ocean only) and MODIS using the Neural Net Retrieval algorithm. AVHRR assimilation ended in August 2002, when MODIS Aqua assimilation began. MISR (Multi-angle Imaging Spectroradiometer) and AERONET observations were assimilated until June 2014 and October 2014, respectively. AOD(550) is the only aerosol product in MERRA-2 directly constrained by the

data assimilation system (Randles et al., 2017), while speciated AODs are indirectly constrained through total AOD assimilation, which helps mitigate the impact of outdated emission inventories (see Appendix 1).

This study used monthly mean AOD(550) and speciated AODs (GMAO, 2015a), while hourly data were used for evaluation in Appendix 3 (GMAO, 2015b), and monthly mean wind speed at 50 m above sea level was used in the analyses in Section 4.4.5 (GMAO, 2015c).

2.1.2 CAMSRA

The Copernicus Atmosphere Monitoring Service (CAMS) Reanalysis (CAMSRA), produced by the European Centre for Medium-Range Weather Forecasts, provides a global dataset of atmospheric composition species, including aerosols, from 2003 onward (Inness et al., 2019). The CAMSRA data have a spatial resolution of 0.7° × 0.7° and a 3 h temporal resolution. The CAMS meteorological model is based on the Integrated Forecast System (IFS) version cy42r1 (with modifications), with interactive ozone and aerosol in the radiation scheme.

The CAMS aerosol module (Morcrette et al., 2009, with changes documented in Inness et al., 2019) is a hybrid bulk–bin scheme with 12 prognostic tracers. It simulates sea salt (3 size bins), dust (3 size bins), black carbon, sulphate aerosol, hydrophilic and hydrophobic organic matter (OM), and a gas-phase sulphur dioxide (SO_2) precursor. The modelling of aerosols in CAMSRA is presented in Appendix 1.

The total AOD is constrained by assimilation of total AOD(550) observations from AATSR/Envisat (the Advanced Along-Track Scanning Radiometer, 2003–2012), MODIS/Terra and MODIS/Aqua (collection 6, 2003–present) using the 4D variational data assimilation system of the IFS.

This study employed monthly means of total AOD(550) and speciated AODs from CAMS global reanalysis (EAC4) (Inness et al., 2019; CAMS, 2020a); 3-hour data were used for evaluation (CAMS, 2020b), presented in Appendix 3.

Microphysical and optical properties of both reanalyses are summarised in Xian et al. (2024), while worldwide validation of CAMS and MERRA-2 reanalysis AOD products against AERONET observations was performed by Gueymard and Yang (2020).

2.2 Fire data

Fire activity in the Baltic region was characterised using NASA's Fire Information for Resource Management System (FIRMS) (https://www.earthdata.nasa.gov/data/tools/firms; accessed on 10 September 2024), part of NASA's Earth Science Data and Information System (ESDIS). MODIS Collection 6.1 fire detection (2001–2023) was used.

In this study, the number of fires in a given sector was obtained as follows: only hotspots with a quality flag > 60% were included; detections within 1 km on the same day were treated as a single fire, while multi-pixel fires were counted per pixel; and fires persisting over several days were counted daily. It should be noted that the number of fires does not precisely indicate actual emissions, which may vary depending on vegetation type, fire phase and intensity. A quality threshold of 60% was adopted as a compromise between maximising fire detection and minimising false positives. Lower threshold values increase the likelihood of detecting all active fires but also introduce a higher rate of false detections, whereas higher threshold values improve detection confidence but may exclude weaker or less certain fire signals.

2.3 NAO index

In this study, the temporal variability of atmospheric circulation is represented by the North Atlantic Oscillation (NAO) index. It is based on the difference in sea-level pressure between the Icelandic Low and the Azores High (Meier et al., 2023). During the positive phase of the NAO, pressure in the northern part of the North Atlantic is below average, while in the central part it is above average. During the negative phase, the pressure pattern is reversed. The NAO influence on European climate is strongest in winter, when it modulates westerly circulation, precipitation, and storminess across northern Europe (Meier et al., 2022).

Monthly NAO index values used in this study were obtained from the Climate Prediction Center database of the NOAA National Centers for Environmental Prediction (https://www.cpc.ncep.noaa.gov/products/precip/CWlink/pna/norm.nao.monthly.b5001.current.ascii.table; accessed on 5 November 2024), and computed using rotated principal component analysis (RPCA) following Barnston and Livezey (1987) (https://www.cpc.ncep.noaa.gov/data/teledoc/teleindcalc.shtml; last access: 17 October 2025).

3. Methods

In this study, the Baltic Sea was divided into six sectors (s1–s6), each defined as a 1°× 1° latitude-longitude grid cell, as shown in Figure **??**. Two additional composite sectors were defined: a northern sector (sN) comprising s1 and s2, and a southern sector (sS) covering the area of s5 and s6. This division enables analyses of both meridional (south–north) and zonal (east–west) variability in AOD over the Baltic Sea. Total and speciated AOD values for each sector were calculated as area-weighted means of all reanalysis grid cells within the sector.

Because CAMSRA covers a shorter period than MERRA-2, two intervals were analysed separately: 1980–1999 (MERRA-2 only) and 2003–2023 (MERRA-2 and CAMSRA). Changes in observing-system inputs around 2000–2002 improved MERRA-2 AOD constraints, resulting in differences between the periods in assimilated observations and satellite detections used for fire emission inventories.

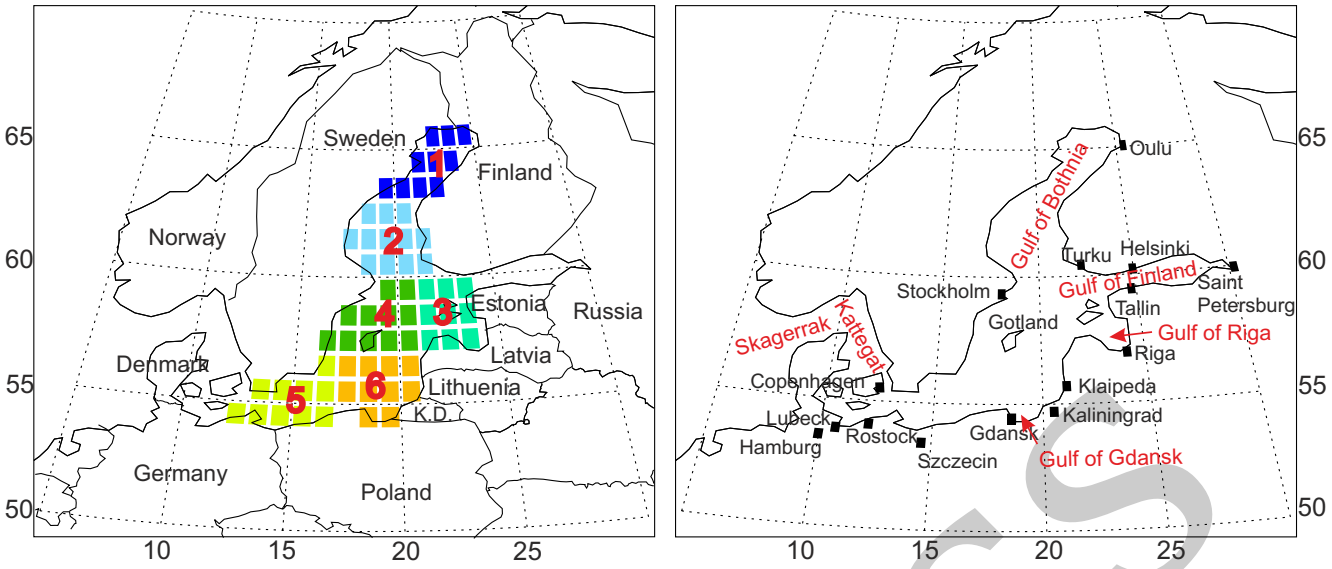

Figure 1. Division of the Baltic Sea into sectors used in this study to analyse aerosol optical depth (left panel) and location of gulfs and straits mentioned in this study (right panel). K.D. stands for Kaliningrad District.

The statistical significance of trends and their slopes was assessed using the non-parametric Mann–Kendall test and the associated Sen's slope estimator, both with autocorrelation correction following the 3PW (three prewhitening) algorithm of Collaud Coen et al. (2020). This approach does not assume normally distributed data and properly accounts for autocorrelation in the time series. The null hypotheses of no trend were tested at significance levels of 0.10 and 0.05. Accordingly, in the following, ss90 and ss95 denote trends that are statistically significant at the 90% and 95% confidence levels, respectively, while ns indicates a non-significant trend. Trend values are reported in the form: slope [lower bound; upper bound], where the values in brackets represent the 62% confidence intervals of the Sen's slope estimate.

4. Results and discussion

4.1 Spatial climatology of AOD(550)

Mean AOD values averaged over the entire Baltic Sea are 0.221 ± 0.012 (mean and standard deviation of the mean due to interannual variability) for MERRA-2 (1980–1999), 0.135 ± 0.002 for MERRA-2 (2003–2023), and 0.116 ± 0.003 for CAMSRA (2003–2023). In Sections 4 and 5, AOD refers to AOD(550).

The surface distribution of AOD over the Baltic Sea is characterised by a nearly meridional (SSE–NNW) decrease in AOD (Figure **??**). Except for lower AOD values in the 2003–2023 period compared to 1980–1999, the surface distribution patterns are very similar for both averaging periods and both reanalyses. The highest AOD occurs over the southeastern Baltic (s6) during 1980–1999 and over the southwestern sector (s5) thereafter, with a minimum

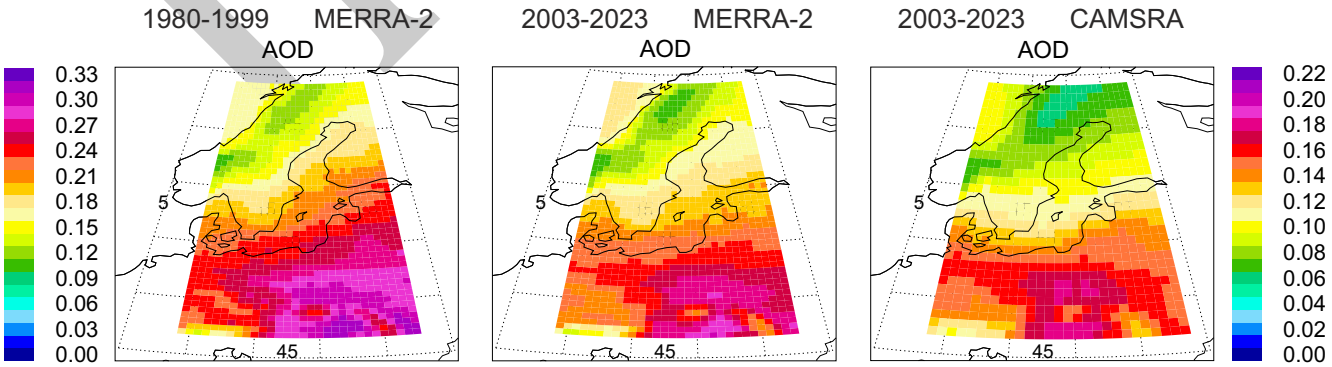

Figure 2. Long-term mean distributions of total AOD(550) in the Baltic Sea region based on MERRA-2 data for the periods 1980–1999 (left) and 2003–2023 (middle) and on CAMSRA data for the period 2003–2023 (right). The colour bar on the left applies to the left graph only.

in s1 for all cases. For 2003–2023, the south–north AOD gradient is slightly stronger in CAMSRA (ΔAOD = –0.053) than in MERRA-2 (ΔAOD = –0.039).

This spatial pattern agrees with previous studies (Mancinelli et al., 2024) and reflects the southern location of the main anthropogenic aerosol sources. The differences between the reanalyses can be attributed to different methods and, in part, to different data sources used in data assimilation.

Spatial patterns for speciated AODs largely follow the total AOD distribution, except for sea salt and organic components (Figure **??**). Sea-salt AOD (AOD_SS) decreases from the Skagerrak-Kattegat toward the Gulf of Bothnia and Gulf of Finland (Table A3). Basin-wide means are $0.020 \pm$
0.0005, 0.019 ± 0.0004, and 0.018 ± 0.0005 for MERRA-2 (1980–1999), MERRA-2 (2003–2023), and CAMSRA (2003–2023), respectively. CAMSRA exhibits a steeper gradient along the Baltic Sea but a weaker inland decline, suggesting less efficient sea-salt removal than in MERRA-2.

Organic aerosol AOD (AOD_OC/AOD_OM) shows the largest differences between the reanalyses (Figure **??**c). In MERRA-2 (1980–1999), AOD_OC decreases east–west, whereas after 2003 it becomes nearly uniform, with only $\sim 9\%$ variation between sectors. CAMSRA, however, exhibits a typical south–north gradient (maximum in s5, minimum in s1) with 40% variation.

The basin-wide mean AOD_OC values from MERRA-2 for the periods 1980–1999 and 2003–2023 are close to each other (0.019 ± 0.001 and 0.021 ± 0.001, respectively) but more than a factor of two lower than the CAMSRA AOD_OM (0.055 ± 0.002), which is consistent with the global ratio (~ 2.3) reported by Xian et al. (2024). A significant overestimation of surface concentrations of organic matter from the CAMS global forecasting system has been noted when compared with SPARTAN network data (Surface PARTiculate mAtter Network; Amarillo et al., 2024). It should be noted that CAMSRA OM and MERRA-2 OC are not directly comparable optical proxies, as OM includes oxidation products and secondary organic aerosol, whereas OC represents only primary carbonaceous material.

Black carbon AOD (AOD_BC) also follows a meridional gradient (Figure **??**d). In MERRA-2 (1980–1999), AOD_BC decreases from s6 to s1 by $\sim 44\%$; in 2003–2023, the relative difference is 46% for MERRA-2 and 41% for CAMSRA, both with maxima in s5. Mean basin values are 0.0069 ± 0.0002, 0.0074 ± 0.0001, and 0.0058 ± 0.0009 for MERRA-2 (1980–1999), MERRA-2 (2003–2023) and CAMSRA (2003–2023).

Sulphate AOD (AOD_SU) exhibits a clear SSE–NNW decrease similar to total AOD (Figure **??**e), with inter-sector differences of 32–41%. However, absolute values differ greatly. The basin means are 0.160 ± 0.011, 0.069 ± 0.002, and 0.033 ± 0.001 for the three datasets, meaning CAMSRA values are roughly half those of MERRA-2. Xian et al. (2024) reported that the AOD_SU values derived from CAMSRA are lower than those from MERRA-2 for Europe, Asia and America. The discrepancies are linked to differences in emission inventories. For example, SO2 emissions from AeroCom (previous version) used in MERRA-2 are about twice those in MACCity (CAMSRA) over Europe in the period 2000–2006 (Granier et al., 2011).

Dust AOD (AOD_DU) peaks in s6 (MERRA-2) or s5–s6 (CAMSRA) and is minimal in s1. Spatial contrasts are $\sim 32\%$ for both MERRA-2 periods but $\sim 94\%$ for CAMSRA (Figure **??**b). Basin-mean values are 0.016 ± 0.0006, 0.018 ± 0.0006, 0.004 ± 0.0002 (MERRA-2 1980–1999, MERRA-2 2003–2023, CAMSRA 2003–2023). The significantly higher dust AOD from MERRA-2 agrees with Xian et al. (2024). They found large differences between the two reanalyses for the Sahara, the main source of the desert dust over Europe, and the deserts of Central Asia and the Arabian Peninsula, locally exceeding 0.05. However, they attributed differences in AOD_DU from MERRA-2 and CAMSRA over regions distant from the main sources to differences in dust removal processes between the reanalyses.

Detailed characterisation of total and speciated AOD spatial distributions is given in Table A3.

4.2 Trends

4.2.1 1980–1999

Over the 40+ years covered by the MERRA-2 reanalysis (Figure **??**) and the 20+ years covered by the CAMSRA (Figure **??**), both total AOD values and values of speciated AODs vary significantly. Over the last two decades of the 20th century, the annual mean AOD averaged for the entire Baltic Sea decreased at a rate of 0.073 [−0.111; −0.045] per decade (ss90; Figure **??**). The decline is strongest in the central and southern Baltic Sea (s4–s6: −0.07 to −0.08 1/10y; ss90) and weakens northward (s1–s2: −0.055 to −0.060 1/10y; ss95). Trends for monthly means varied depending on the month and sector, with the largest decreases in May (basin-mean trend: −0.096 [−0.157; −0.031] 1/10y; ns) and March (−0.091 [−0.13; −0.057] 1/10y; ss90). South–north contrasts in trend values are pronounced in June and July.

Trends in 1980–1999 reflect a gradual reduction in anthropogenic emissions (de Meij et al., 2012), mainly sulphates and sulphur oxides, driven by EU regulations, economic crisis and a political transformation (“perestroika”) in Central and Eastern Europe. “Perestroika” began in the mid-1980s and was associated with a partial industrial decline and changes in pollutant emission limits. The observed trends are also influenced by two strong volcano volcanic eruptions (El Chichón, 1982; Pinatubo, 1991), visible as 1983 and 1992 AOD peaks in Figure **??**, and a decrease in volcanic activity after 1991 (Markowicz et al., 2022). It must be noted that the trend estimates include these high-AOD years, which likely enhances the apparent magnitude of the negative trend but decreases its statisti-

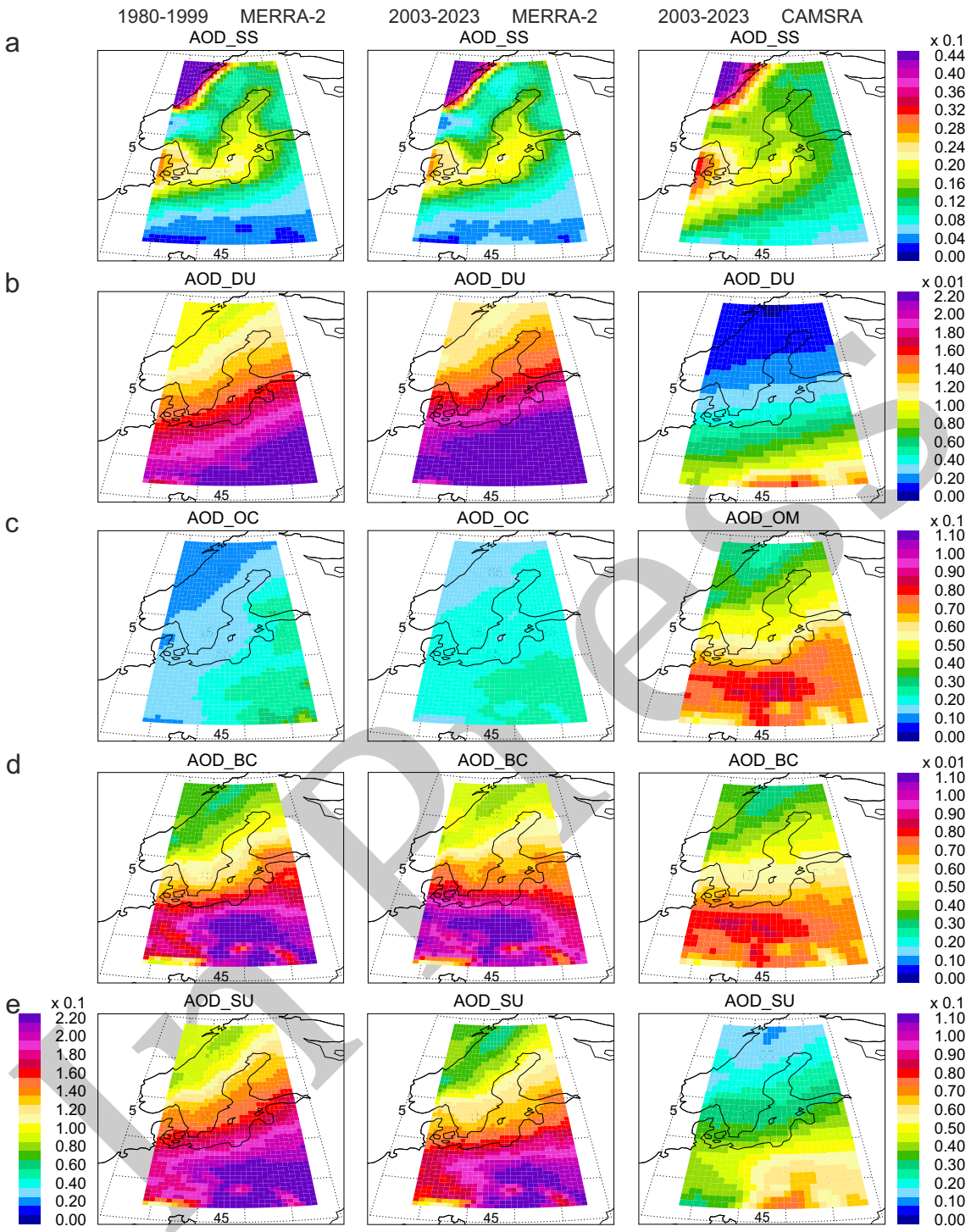

Figure 3. Spatial distributions of speciated AOD(550) from MERRA-2, averaged over the periods 1980–1999 and 2003–2023, and from CAMSRA, averaged over the period 2003–2023. The left colour bar refers to AOD_SU from MERRA-2 for the period 1980–1999. Scale values should be multiplied by the appropriate multipliers given above the colour bars.

cal significance. Trends in the total AOD generally agree with the corresponding trends in the AOD_SU (Figure **??**a).

In 1980–1999, all the statistically significant trends, both for annual means of total and speciated AODs and for the monthly means, were negative. The positive AOD_SS trend in February (ss95) and March (ss90; Figure **??**) is an exception and aligns with a late-winter and early-spring wind intensification and autumnal weakening over

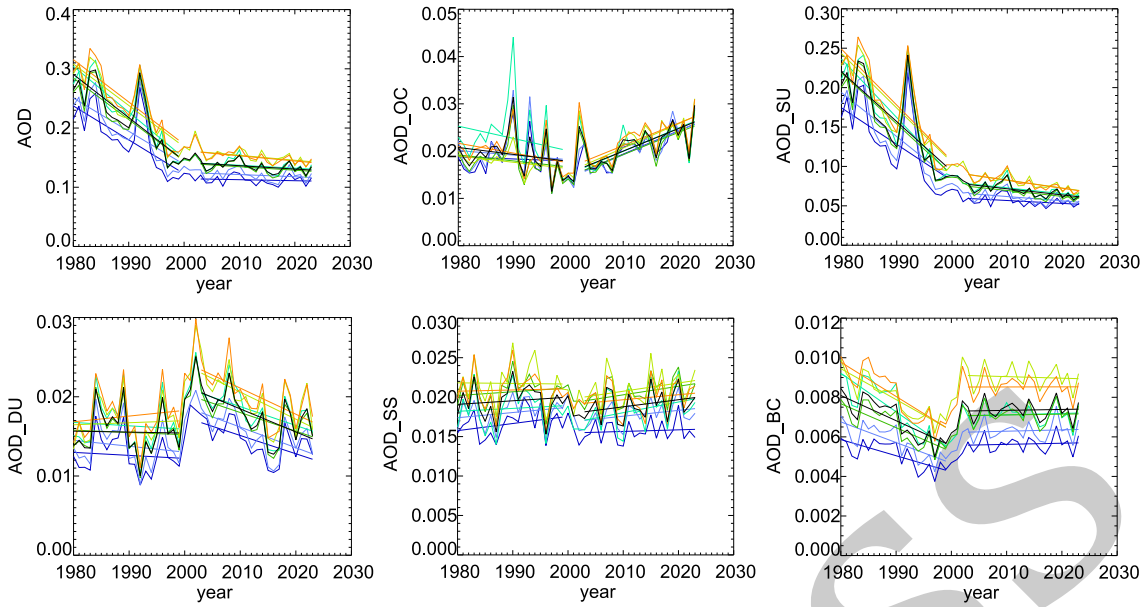

Figure 4. Temporal variability of annual spatial means of AOD and speciated AODs from MERRA-2 for the entire Baltic Sea (black) and the sectors (colours indicate sectors as in Figure **??**). Straight lines represent the corresponding trends for the periods 1980–1999 and 2003–2023.

1970–2007 (Lehmann et al., 2011).

4.2.2 2003–2023

In the 21st century, the reduction rate in anthropogenic emissions is much lower (Figure A2 in Mancinelli et al., 2024) and the impact of volcanic activity on atmospheric aerosol in Europe is weaker, which results in weaker AOD trends. The trend for the annual basin-mean AOD is −0.0056 [−0.0094; −0.0020] 1/10y (−4.2%/10y) and statistically insignificant for the MERRA-2 data and −0.0156 [−0.021; −0.0087] 1/10y (−11.6%/10y) and statistically significant (ss90) for the CAMSRA data. These

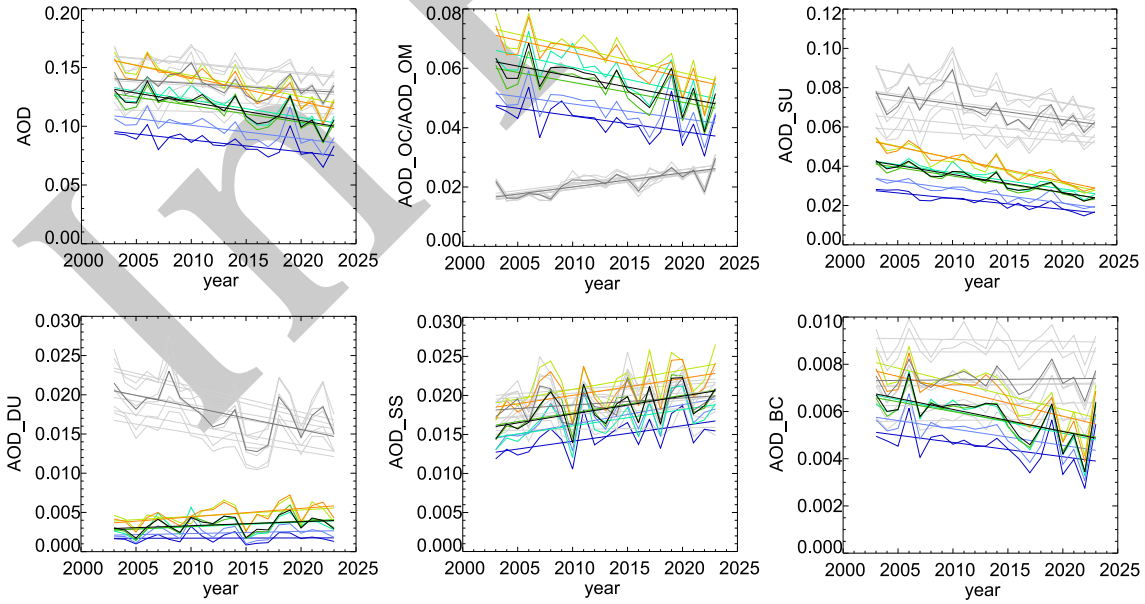

Figure 5. Temporal variability of annual spatial means of AOD and speciated AODs from CAMSRA for the entire Baltic Sea (black) and the sectors (colours indicate sectors as in Figure **??**). Straight lines show the corresponding trends for the period 2003–2023. The corresponding time series of total AOD and speciated AODs from MERRA-2 (from Figure **??**) are plotted in grey for comparison.

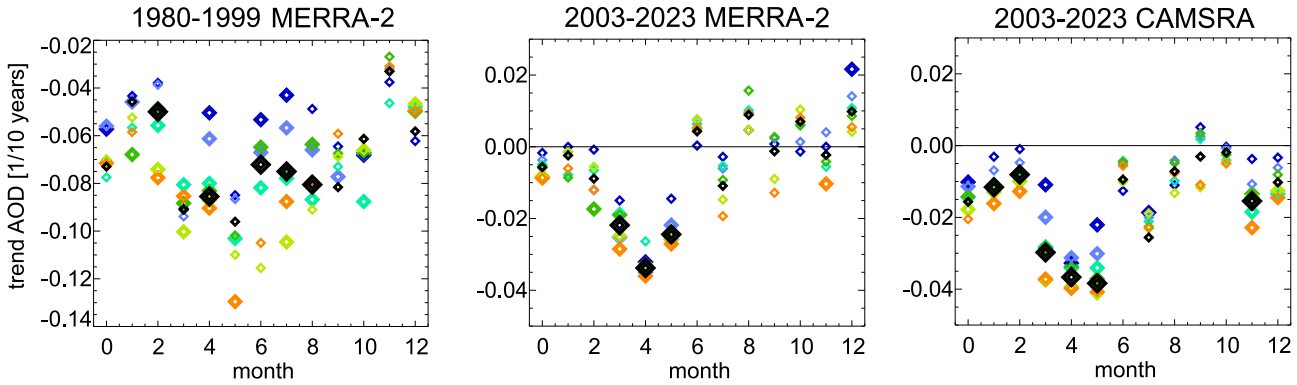

Figure 6. Seasonal variations in trends in monthly mean AOD for selected sectors and the entire Baltic Sea. Colours indicate sectors (see Figure **??**), black colour indicates trends in means for the entire Baltic Sea, month=0 indicates trends in annual means, and larger symbols indicate statistically significant trends at a significance level of 0.05. Individual graphs show trends for different periods: 1980–1999 (left), 2000–2023 (middle) and 1980–2023 (right).

values are comparable to the AOD(550) trend of −0.0084 1/10y (−5.6%/10y) determined by Han et al. (2025), based on MODIS measurements in the years 2001–2023 over the entire Baltic Sea.

The trends remain more negative in the southern sectors, with the highest magnitudes in s6 for MERRA-2 (−0.0087 [−0.0123; −0.0057] 1/10y, −5.8%/10y; s95) and for CAMSRA (−0.0205 [−0.032; −0.014] 1/10y, −15.1%/10y; ns). The weakest trends are found in s1: −0.0017 [−0.00546; 0.0029] 1/10y (−1.5%/10y; ns) for MERRA-2 and (−0.0101 [−0.0108; −0.0084] 1/10y, −11.9 %/10y; ss95) for CAMSRA. Despite both systems assimilating AOD, CAMSRA trends in annual mean AOD are at least twice as negative as MERRA-2 across most sectors, which can be attributed to partly different data sources used in data assimilation in the reanalyses and different assimilation algorithms (compare Sections 2.1.1 and 2.1.2).

Previous studies also indicate a meridional decrease in the trend magnitude over the Baltic Sea. According to Glanz et al. (2019), the trends are −0.024 1/10y for the southwestern Baltic Sea (MODIS Collection C061; 2003–2017, April to September) and −0.017 1/10y for the western Gotland Basin in Sweden. An increase in the trend value northward is also observed on a larger scale. Han et al. (2025) reported trends for the Northern Europe sector of −0.0013 1/10y (−0.9%/10y), +0.0023 1/10y (1.7%/10y) for Svalbard and +0.0070 1/10y (5.5%/10y) for the Greenland Sea sector, compared to −0.0084 1/10y (−5.6%/10y) for the Baltic Sea sector. The Northern Europe sector extends farther west and north than the Baltic Sea sector in Han et al. (2025).

For MERRA-2, AOD trends for individual months are predominantly negative from January to May and predominantly positive from June onward. The trends are mostly statistically insignificant. Statistically significant trends (ss95) are only observed in March, April and May, with the largest decrease in April (−0.034 [−0.046; −0.022] 1/10y) for the whole Baltic Sea. In the case of CAMSRA, trends for individual months are predominantly negative throughout the year. More months show statistically significant trends than for MERRA-2. Statistically significant trends (ss95) are observed for the periods January to May and November, with the largest decrease observed in April and May (−0.037 [−0.047; −0.024] and −0.038 [−0.054; −0.017] 1/10y). The difference between spring and summer trends (0.03–0.04 1/10y) is significantly lower than those reported by Han et al. (2025) for the Baltic Sea (−0.116 1/10y in spring; +0.025 1/10y in summer).

According to the MERRA-2 reanalysis, the statistically significant negative trends in total AOD in spring coincide with negative trends in AOD_SU and AOD_DU. In CAMSRA, the strongest decreases in total AOD in May and April are accompanied by negative trends in AOD_SU and AOD_OM, representing a key difference compared to MERRA-2. In both reanalyses, April AOD is strongly correlated with fire activity in the Baltic region (Section 4.3.4), suggesting that the observed April decrease is associated with a reduction in agricultural burning. However, CAMSRA attributes a larger organic fraction to fires than MERRA-2 (Section 4.3.4).

In the case of the trends in speciated AODs, only indirectly constrained by data assimilation, significant differences can be observed between aerosol species and the reanalyses (Figure **??**):

1. The trends in annual means of AOD_SU are negative and similar across reanalyses (basin-mean trend: −0.0078 [−0102; −0.0053] 1/10y, ss95, for MERRA-2 and 0.0092 [−0.0147; 0.00166] 1/10y, ss90, for CAMSRA). The trend values are mostly negative in both seasonal cycles. Seasonal extremes occur in April for MERRA-2 (−0.025 [−0.033; −0.021] 1/10y, ss95) versus July for CAMSRA (−0.020 [−0.022; −0.015] 1/10y, ss95) (Figure **??**c).

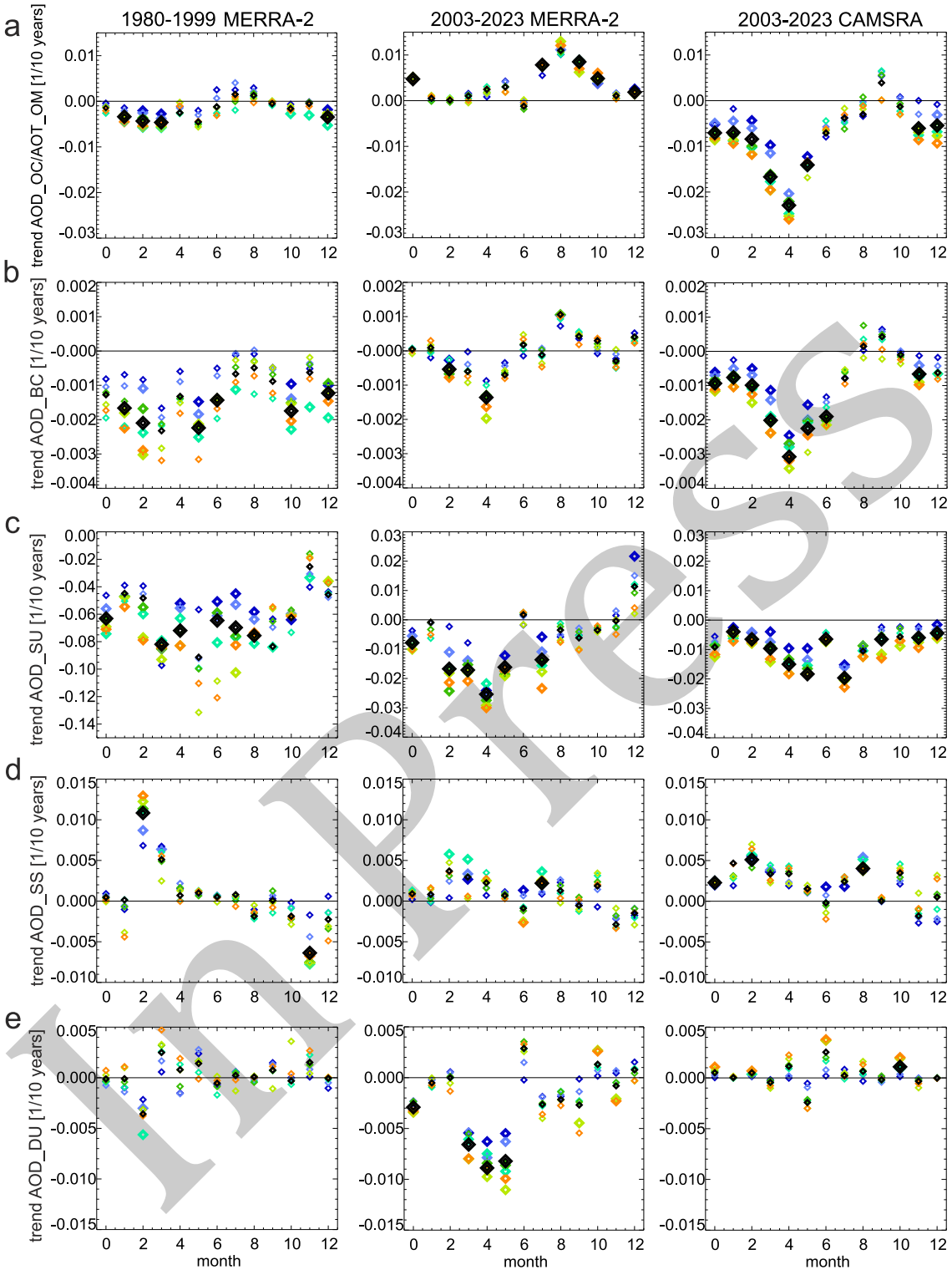

Figure 7. Seasonal changes in trends in monthly mean speciated AOD: (a) AOD_OC, (b) AOD_BC, (c) AOD_SU, (d) AOD_SS, and (e) AOD_DU, for selected sectors and the entire Baltic Sea. Colours indicate sectors (see Figure **??**), black indicates trends in the means for the entire Baltic Sea, month=0 indicates trends in annual means, and larger symbols indicate trends statistically significant at a significance level of 0.05. Columns show trends for different periods: 1980–1999 (left), 2000–2023 (middle) and 1980–2023 (right).

2. The trends in annual basin means of AOD_OC/OM from MERRA-2 and CAMSRA are statistically significant and opposite: positive for MERRA-2 (0.0047 [0.0034; 0.0058] 1/10y, s95) and negative for CAMSRA (−0.0071 [−0.0094; −0.0056] 1/10y, ss95) (Figure **??**a). Maximum seasonal trend values occur in late summer and early autumn: a statistically significant positive trend of 0.011 [0.0057; 0.017] 1/10y (ss90) in August for MERRA-2 and insignificant +0.0039 [−0.0031; 0.0090] 1/10y in September for CAMSRA. Surface OC concentration at Utö marine station (2011–2021) shows a strong decrease (Friman et al., 2023), closer to CAMSRA than MERRA-2, noting that AOD integrates elevated layers.

3. The trend of AOD_BC annual basin-means from CAMSRA is near zero in MERRA-2 (−0.00005 [−0.00016; 0.00022 1/10y, ns) and negative in CAMSRA (−0.00094 [−0.0012; −0.00050] 1/10y, ss95). Seasonally, both show a spring depression and late-summer crest; in April the trends are −0.0014 [−0.0020; −0.00089] (MERRA-2, ss95 ns) and −0.0031 [−0.0035; −0.0024] per decade (CAMSRA, ss95), with late-summer values peaking in August/September (0.0011 [0.0004; 0.0016] 1/10y, ss90, and 0.0004 [−0.00023; 0.0009] 1/10y, ns) (Figure **??**b). A negative but statistically insignificant trend in surface elemental carbon concentration was observed at the Utö marine station between 2011 and 2021 (Friman et al., 2023).

4. AOD_SS trends are predominantly positive, but mostly statistically insignificant (Figure **??**d). The trend in annual means averaged over the entire Baltic Sea is 0.0009 [0.00009; 0.0016] 1/10y (ns) in the case of MERRA-2 and 0.0023 [0.0013; 0.0033] 1/10y (ss95) for CAMSRA. Like in the period 1980–1999, the largest monthly increases occur in February in both reanalyses (MERRA-2: 0.0037 [0.0012; 0.0068] 1/10y, ns; CAMSRA: 0.0051 [0.0031; 0.0082] 1/10y, ss95).

5. AOD_DU trends from MERRA-2 and CAMSRA data show different seasonal cycles (Figure **??**e). MERRA-2 shows a significant negative annual trend (−0.0029 [0.0045; −0.0012] 1/10y; ss95), driven by spring (−0.009 to −0.006 1/10y). CAMSRA trends are weak and statistically insignificant (annual mean trend: −0.0005 [0.00012; 0.0009] 1/10y, ns), with an isolated significant October increase (0.0011 [0.0008; 0.0016] 1/10y, ss95) (Figure **??**e).

4.3 Seasonality

Spatial and seasonal variation in trends of the total and speciated AODs have led to long-term temporal and spatial variability in seasonal AOD cycles (Figure **??**). Decadal seasonal cycles of total AOD evolve from a single spring peak in 1980–89 (March, sector sN; May, sector sS) to a double-peak pattern in 2003–2023 with the maxima in April/May and July/August. Starting from the decade 1980–1999, the decadal mean AOD and the amplitude of seasonal changes decline, mainly due to spring decreases. The summer maximum declines more gradually in CAMSRA and remains largely persistent in MERRA-2, becoming the dominant feature of the seasonal cycle during 2013–2023. MERRA-2 consistently shows a smaller annual amplitude of AOD variability compared with CAMSRA, consistent with findings reported for Europe by Xian et al. (2020, Supplement). In both reanalyses, seasonal AOD variability is weaker over the northern Baltic Sea sector (sN).

In the 2013–2023 decade, the MERRA-2 monthly mean AOD ranges from 0.092 (October) to 0.131 (August) in sN and from 0.113 (December) to 0.175 (August) in sS. CAMSRA mean AOD ranges from 0.040 (January) to 0.142 (August) in s1 and from 0.061 (December) to 0.192 (July) over the southern Baltic Sea. A comparison of the seasonal cycles from MERRA-2 and CAMSRA with the seasonal cycle from the AERONET Helsinki station (2009–2023) indicates that MERRA-2 reproduces the cycle shape better, but consistently overestimates the long-term monthly means (Appendix 3, Figure A3).

The main features of the seasonal cycles of speciated AODs are as follows:

1. The seasonal variability of AOD_SS differs from that of the other AOD components. For all decades and regions (sN, sS), the MERRA-2 AOD_SS cycle shows a minimum in May (0.008–0.013) and a maximum in winter (January or December; 0.026–0.039), matching wind seasonality. CAMSRA shows larger AOD_SS values than MERRA-2 from March to May, resulting in the minimum AOD_SS in July (0.008–0.014) and the maximum in December (sN; 0.022–0.028) and January–February (sS; 0.027–0.031).

2. The seasonal cycles of MERRA-2 and CAMSRA AOD_DU show the same trend – an increase in AOD_DU in June relative to AOD in April and May. In the 2013–2023 decade, the CAMSRA AOD_DU maximum was found in June (0.005/0.012 for sN/sS) and the MERRA-2 in April (0.025/0.036 for sN/sS), but AOD_DU in June is greater in 2013–2023 than in the previous decade. The minimum AOD_DU is found for winter in both reanalyses.

3. The main features of long-term changes of the seasonal cycle of AOD_SU over the Baltic Sea are a flattening, i.e., a reduction in amplitude, and the disappearance of the spring maximum. These features occur in the southern Baltic Sea (sS) and the Gulf of Bothnia (sN) in both reanalyses. However, the flattening of the seasonal cycle is stronger in the

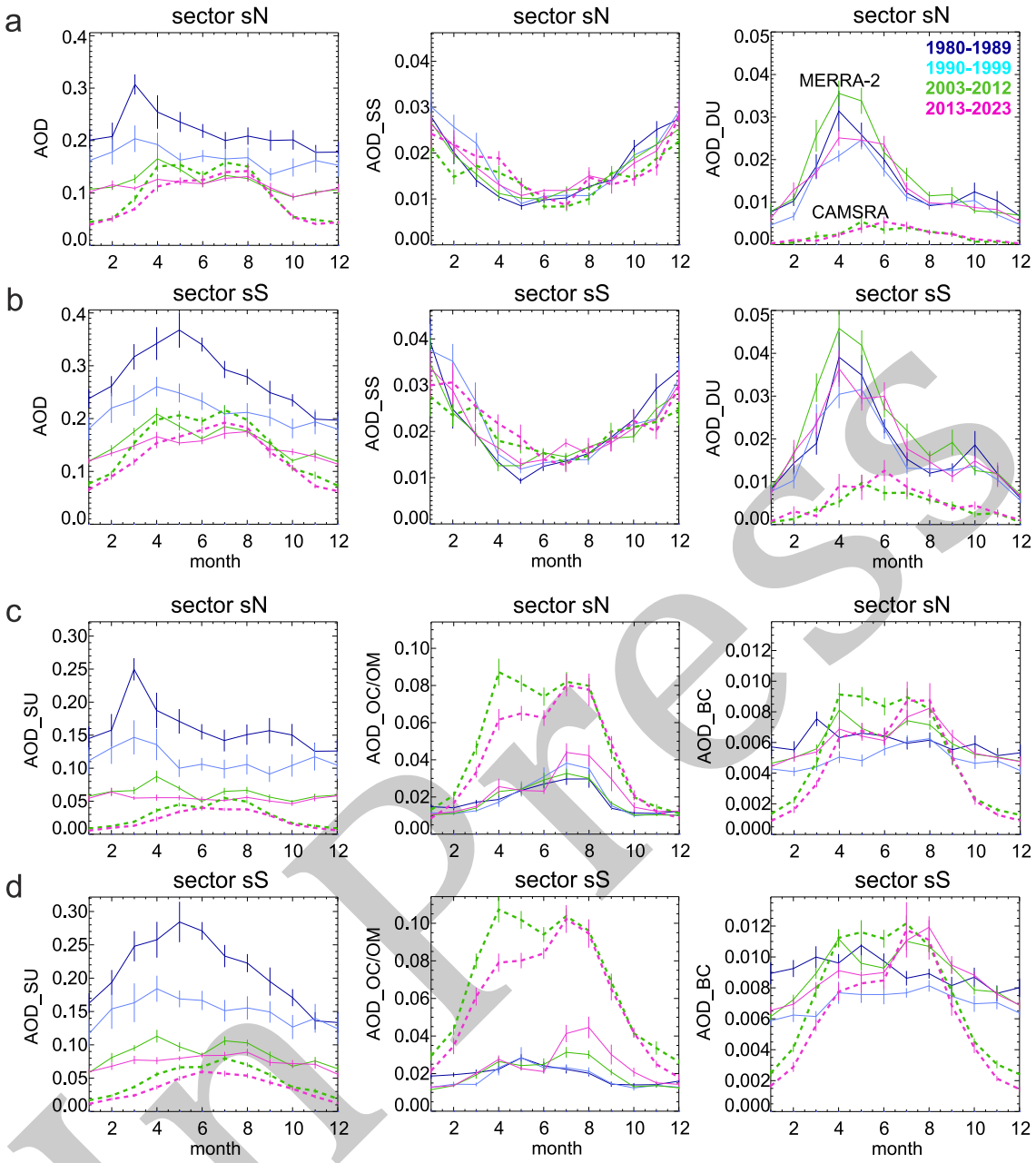

Figure 8. Decadal mean annual cycles of (a, b) AOD and AOD components: AOD_SS and AOD_DU, and (c, d) AOD_SU, AOD_OC, and AOD_BC, for (a, c) the northern part of the Baltic Sea (sN) and (b, d) the southern part of the Baltic Sea (sS). Colours indicate decades. Dashed lines indicate results from CAMSRA, and solid lines indicate results from MERRA–2.

MERRA-2 case. In the case of MERRA-2, for the period 2013–2023, the decadal monthly mean AOD_SU ranges from 0.053 in October to 0.063 in February in sN and from 0.056 in December to 0.089 in August in sS. For CAMSRA, the mean AOD_SU value ranges from 0.006 (January) to 0.041 (June) in sN and from 0.011 (January) to 0.060 (June) in sS.

4. In the late 20th century, the seasonal distribution of AOD_OC shows a single peak, in July/August (sN) or May (sS). In the 2000s, a transition to bi-peak cycles was observed. In the period 2013–2023, both reanalyses yield a maximum in summer in both sectors (MERRA-2: 0.044/0.045 in sN/sS; CAMSRA: 0.081/0.102). As mentioned earlier, the AOD_OC from MERRA-2 shows a W-E gradient or uniform surface distribution, therefore differences between decadal monthly means are small between the sN and sS sectors. Summer maxima match the seasonal cycle of surface organic carbon concentration at the Utö marine station

in Finland (2011–2021) with a peak in July (Friman et al., 2023). The summer maximum was also observed at Arctic and rural sites in Finland, which Friman et al. (2023) attributed to a dominant role of secondary organic aerosol formation, mainly from biogenic precursors.

5. Similar to AOD_OC/OM, the seasonal distribution of AOD_BC has changed from a single-peak cycle to a double-peak pattern, with maxima in April/May and July/August and a minimum in winter (December, January). In the decade 2013–2023, the summer maximum becomes dominant in both reanalyses (0.008–0.009/0.012 in sN/sS). No clear seasonal variations of surface elemental carbon concentration were observed at the Utö marine site (Friman et al., 2023).

Temporal variations of species contributions to total AOD are presented in Appendix 4. Unlike AODs, the contributions or ratios of a speciated AOD to the total AOD are unconstrained by AOD assimilation.

4.4 Long-term AOD fluctuation analysis

In this section, we analyse the consistency of the reanalyses in reproducing temporal AOD variability, spatial coherence of AOD variability, the spatial differentiation of AOD fluctuation amplitudes, and correlations of AOD variability with the NAO index and fire activity in the Baltic Sea region.

4.4.1 Reanalysis consistency

To analyse the extent to which both reanalyses are consistent in reproducing the temporal variability of total and speciated AODs, correlation coefficients were calculated between the detrended annual and monthly AOD means from MERRA-2 and CAMSRA data for the Baltic Sea area (Table A4). The correlation coefficient for annual means of total AOD was 0.75. The best agreement between the speciated AOD variability from MERRA-2 and CAMSRA was obtained for AOD_BC (0.83), AOD_SS (0.72) and AOD_OC/AOD_OM (0.64). The corresponding correlation coefficients for AOD_DU and AOD_SU are 0.53 and 0.47. All these correlation coefficients are statistically significant at a significance level of 0.05. The best agreement was obtained for the total AOD, constrained by assimilation of measured AOD, AOD_BC, determined daily from satellite observations, and AOD_SS estimated mainly from wind speed. The good agreement in total AOD is partly expected, as both reanalyses assimilate MODIS data. Dust aerosol emission is also wind-speed dependent, but major dust sources are located far from the Baltic Sea, which makes AOD_DU over the Baltic Sea susceptible to many processes, e.g., the height of the dust injection to the atmosphere and removal processes on the transport path from the sources to the Baltic Sea.

The correlation coefficients between AODs from MERRA-2 and CAMSRA vary seasonally. Even for aerosol components with relatively low correlation coefficients for annual means, such as dust and sulphate aerosols, correlations can be seasonally significant. AOD_SU shows the highest correlation coefficient from April to July (0.68–0.84), while summer and autumn are periods with relatively high correlation for AOD_DU (> 0.73). The correlation coefficients between detrended total AOD strongly depend on the availability of data for assimilation and are lowest for December and January.

4.4.2 AOD north-south coherence

Another question regarding the spatial and temporal variability of monthly mean AOD is whether AOD fluctuations (deviations from the trend line) occur simultaneously over the entire Baltic Sea. To assess this, correlation coefficients between detrended AOD and speciated AODs over the northern (sN) and southern (sS) parts of the Baltic Sea were calculated based on MERRA-2 and CAMSRA data (Table A5). For the detrended annual means, the correlation coefficients are high and largely comparable: 0.79–0.87 for MERRA-2 and 0.60–0.89 for CAMSRA. Significant differences between the reanalyses occur for AOD_SU and AOD_DU, where the CAMSRA correlation coefficients are lower by about 0.25.

The seasonal cycles of correlation coefficients between detrended monthly means of total AOD over the northern and southern Baltic Sea from both reanalyses are also comparable and show similar month-to-month variability (Table A5). The lowest correlation coefficients were obtained for March (statistically insignificant for both reanalyses) and October (statistically insignificant for MERRA-2 and 0.44 for CAMSRA), the largest values for July (0.80 and 0.76 for MERRA-2 and CAMSRA, respectively), August (0.80, 0.83) and December (0.80 and 0.74). The low correlation between AOD in sN and sS suggests that the northern and southern Baltic Sea are more often influenced by different aerosol regimes (different air masses).

For speciated AOD, the differences in the corresponding correlations from MERRA-2 and CAMSRA are larger. CAMSRA typically yields higher AOD_SS coherence than MERRA-2, which is consistent with stronger sea-salt transport from the Atlantic Ocean to the Baltic Sea in CAMSRA (compare Figure **??**a).

4.4.3 AOD fluctuation amplitudes

A ratio of the root-mean-square deviations of AOD from the respective trend lines for sectors sN and sS provides information on the proportion of the magnitude of AOD fluctuations relative to the respective trend lines in the northern and southern parts of the Baltic Sea. For the annual means of AOD_SS, AOD_BC, and AOD_DU, both reanalyses indicated a decrease in the magnitude of fluctuations in the south-north direction. The ratios were 0.78 and 0.67 for AOD_DU (from MERRA-2 and CAMSRA, respectively), 0.64 and 0.79 for AOD_SS and 0.86 and 0.96 for AOD_BC. AOD_OC (AOD_OM) shows very similar magnitudes of fluc-

tuations in the southern and northern parts of the Baltic Sea (ratios of 0.97 and 1.07, respectively).

For total AOD and AOD_SU, MERRA-2 and CAMSRA show different patterns – a decrease from south to north for AOD and AOD_SU from CAMSRA (respective ratios of 0.90 and 0.59) and a weak increase or similar magnitude of fluctuations for AOD and AOD_SU from MERRA-2 (ratios of 1.14 and 1.07). It should be noted that despite the higher year-to-year variability in the northern part of the Baltic Sea, the mean AOD clearly decreases from south to north (see also Figures **??** and **??**). Ratios close to 1 suggest a high efficiency of pollutant transport to the northern part of the Baltic Sea during aerosol events such as extensive biomass fires, or short-lived aerosol sources located in the northern Baltic Sea region. As mentioned, due to the Baltic Sea's large meridional extent, different parts can be influenced by different aerosol regimes/air masses. There are cases of pollutants advecting to the northern Baltic Sea, while the southern part is influenced by clean air masses.

4.4.4 Links to fire activity

Wildfires are a significant aerosol source in both reanalyses. We characterise fire activity using the monthly number of FIRMS hotspots (quality $> 60\%$), aggregated over the Baltic region (Figure A5). Months October–February were omitted due to very low counts (monthly maxima < 100), implying negligible direct fire influence on AOD over the Baltic Sea during winter. In the decades 2003–2012 and 2013–2023, fire activity shows a double-peak annual cycle, with maxima in April and August and the minimum in June. In both decades, the highest number of fires in the annual cycle is observed in spring, mainly in April. Spring (April) peaks are dominated by agricultural burning mainly in Russia, the Kaliningrad District, and the Republic of Belarus (with contributions from Ukraine) (McCarty et al., 2016). In summer, the number of fires in the sectors is comparable. The monthly fire count generally declines over time, except for March and October, when it increases in 2013–2023 relative to 2003–2012. The March fire count correlates with the February-March NAO index mean ($R = 0.58$, $p < 0.01$), suggesting warm winters favour earlier agricultural burning and/or natural fires.

The strongest AOD-fire relationships occur in April (Table **??**). Both reanalyses agree on the high correlation ($p < 0.01$) between the fire count and basin-mean total AOD (0.67/0.68 for MERRA-2/ CAMSRA), AOD_BC (0.83/ 0.71), and AOD_SU (0.68/0.66). For organic aerosols, a significant correlation appears only in CAMSRA (0.71), suggesting that CAMSRA attributes a larger organic fraction to fires. Consistently, AOD_BC–AOD_OC/OM correlations are much tighter in CAMSRA (the entire Baltic Sea: 0.95 in April; 0.83–0.95 in May–June) than in MERRA-2 (0.56–0.58).

In April, the correlation coefficients between the fire count and total and speciated AODs are generally higher for sN than for sS, with the exception of AOD_SU from CAMSRA, suggesting that the northern Baltic region with lower anthropogenic backgrounds is more sensitive to episodic pollution transport.

In May and June, the correlations weaken substantially. Despite a secondary fire peak in August, significantly weaker than in spring, summer correlations are mostly insignificant (one exception in Table **??**). This highlights the modulating role of meteorology (specifically transport-wind direction and precipitation) in controlling the impact of fires on AOD.

4.4.5 Links to NAO index

Statistically significant relationships between the NAO index and total and speciated AODs are concentrated in winter (Table **??**). For both reanalyses, AOD_SS correlates positively with NAO, with coefficients decreasing from December (basin mean: 0.77 for MERRA-2; 0.81 for CAMSRA) to February (0.51; 0.54). This is consistent with more frequent westerly circulation and intensification of storm activity over northern Europe and Scandinavia during a positive NAO phase in winter (Meier et al., 2022 and references therein, Meier et al., 2023), enhancing local sea-salt production and advection from the Atlantic. Advection of air masses from the Atlantic is also associated with an increase in air humidity, which may lead to an increase in AOD_SS due to hygroscopic growth.

For other species, the correlations are negative in the winter months. In MERRA-2, AOD_SU is negatively correlated with the NAO index, especially in sector sS (-0.65 in February; -0.77 in December). The correlation with AOD_DU is also negative, but significant only for December (-0.508 for the basin-mean AOD_DU). For CAMSRA, the coefficients between the NAO index and speciated AODs other than AOD_SS are statistically significant only for AOD_BC in February (-0.515 for the basin-mean AOD_BC). These patterns suggest that while positive NAO in winter enhances local sea-salt production, advection from the Atlantic, and possibly the hygroscopic growth of aerosols, the negative NAO phase enhances transport of non-sea salt aerosols to the Baltic Sea. Previous studies have shown that stagnant, cold, and dry high-pressure conditions over the Baltic Sea, associated with a low NAO index, favour pollutant accumulation. In contrast, higher precipitation during high NAO phases enhances wet deposition, particularly of water-soluble particles (Christoudias et al., 2012).

In winter, the reanalyses differ in the sign of the correlation coefficient between total AOD and the NAO index. Statistically significant correlations are positive for CAMSRA and negative for MERRA-2. This discrepancy may result from the limited availability of AOD observations for data assimilation in winter, which leads to less constrained total AOD fields and enhances differences between the models. The opposite signs of the correlation coefficients suggest that the dominant processes through which NAO influences aerosols over the Baltic Sea are different in the

Table 1. Correlation coefficients of total and speciated AOD with the total (in all sectors from Figure A5 combined) monthly fire count around the Baltic Sea for the northern (sN) and southern (sS) Baltic Sea, and the entire Baltic Sea in 2003–2023. Only correlation coefficients statistically significant at a significance level of at least 0.05 are presented. Coefficients significant at a significance level of 0.01 are marked in bold. A slash separates the coefficients for AODs from MERRA-2 (left) and CAMSRA (right).

Month	AOD component	sN	sS	Baltic
3	AOD_BC	–/ –	–/ –	0.44/ –
4	AOD_OC	**–/0.80**	**–/0.61**	–/0.71
	AOD_BC	**0.81/0.85**	**0.78/0.69**	**0.83**/0.80
	AOD_SU	**0.78/0.66**	**0.62/0.69**	**0.68**/0.67
	AOD	**0.78/0.78**	**0.56/0.60**	**0.67**/0.68
5	AOD_OC	–/ 0.51	–/ 0.55	–/0.54
	AOD_BC	–/ **0.56**	**0.56 /0.60**	0.49/ bf 0.60
	AOD_SU	0.47/ –	**0.55/ –**	0.51/–
	AOD	–/–	0.49/ 0.43	–/–
6	AOD_OC	0.51/**0.61**	0.51/0.47	0.52/**0.59**
	AOD_BC	0.54/**0.57**	–/ 0.50	0.51/**0.55**
	AOD	**0.58/0.56**	0.45/ 0.45	**0.59/0.57**
8	AOD_SU	–/–	–/ 0.55	–/ –
9	AOD_SU	–/0.48	–/**0.59**	–/**0.57**

Table 2. Correlation coefficients of total and speciated AOD with the monthly mean NAO index for the northern (sN) and southern (sS) Baltic Sea and the entire Baltic Sea in 2003–2023. Only correlation coefficients statistically significant at a significance level of at least 0.05 are presented. Coefficients significant at a significance level of 0.01 are marked in bold. Slash separates the coefficients for AODs from MERRA-2 (left) and CAMSRA (right).

Month	AOD component	sN	sS	Baltic
1	AOD_SS	**0.57/0.67**	–/**0.62**	0.57/ 0.71
	AOD_SU	–/–	–/–	–/–
	AOD	–/**0.62**	–/**0.47**	–/ 0.55
2	AOD_SS	0.43/**0.59**	0.47/ 0.46	0.51/ 0.54
	AOD_BC	–/–	–/−0.58	–/ −0.52
	AOD_SU	–/–	−0.65/–	−0.57/ –
	AOD	–/–	−0.53/–	–/–
3	AOD_SS	–/ 0.50	–/–	–/–
	AOD_DU	–/ 0.52	–/–	–/ 0.44
7	AOD_SS	–/−0.54	–/−0.61	–/−0.60
8	AOD_DU	–/ 0.48	–/–	–/–
9	AOD_SS	–/ 0.43	–/–	–/–
12	AOD_SS	**0.66/0.74**	**0.76/0.82**	**0.77/0.81**
	AOD_SU	−0.47/–	**−0.77**/–	**−0.65**/–
	AOD_DU	–/–	–/–	−0.51/ –
	AOD	–/0.60	−0.45/–	−0.49/ 0.50

two reanalyses. The positive correlation coefficient between CAMSRA AOD and the NAO index is consistent with a large contribution of AOD_SS to total AOD during the winter months in the CAMSRA reanalysis (compare Appendix 4).

Despite the limited availability of AOD observations in winter, both for assimilation and validation, the correlations between AOT_SS and the NAO index are expected to be robust. In both reanalyses, AOD_SS is closely linked to wind speed (emission) and humidity (hygroscopic growth),

which are routinely measured meteorological variables. Therefore, although absolute AOD_SS values may be biased, their temporal variability is likely to be well represented. In contrast, for other aerosol species, the limited availability of AOD observations in winter may have a stronger impact on the reliability of correlations with the NAO index.

In July, CAMSRA shows a significant negative correlation between AOD_SS and the NAO index (basin: −0.60, sN −0.54, sS −0.61). A negative correlation is also obtained from MERRA-2, but the coefficients are mostly statistically insignificant. This aligns with a negative correlation between the monthly mean wind speed and the NAO index. The value of the correlation coefficient between the monthly basin-mean wind speed (vector mean, MERRA-2) at 50 m above sea level and the NAO index is −0.45 and is statistically significant. This agrees with previous studies (Folland et al., 2009; Dong et al., 2013; Bladé et al., 2012) showing that the variability of storm tracks is closely related to the Summer NAO (SNAO), and the negative phase of the SNAO is associated with a southward shift of storm tracks and their zonal extension, as well as with more extratropical storms moving across the UK and northwestern Europe.

5. Summary and conclusion

Using the results of two reanalyses, MERRA-2 and CAMSRA, we characterised the spatial and temporal variability of AOD over the Baltic Sea, with particular emphasis on differences and similarities between the reanalyses. The study analysed the spatial distributions, trends, and seasonal cycles of total and speciated AOD(550), as well as spatial coherence of AOD temporal variability, spatial changes in amplitudes of AOD fluctuations, and the impact of fires in the Baltic Sea region and the NAO index on the monthly means of AOD. Major highlights of this paper include the following:

1. The long-term means of AOD(550) for the whole Baltic Sea area are 0.221 ± 0.012 (mean and standard deviation of the mean), 0.135 ± 0.002, and 0.116 ± 0.003 for MERRA-2 (1980–1999), MERRA-2 (2003–2023), and CAMSRA (2003–2023), respectively. In the period 2003–2023, the surface distributions of AOD from MERRA-2 and CAMSRA are very similar, except for a slightly higher mean AOD and a stronger south-to-north AOD decrease for CAMSRA (ΔAODMERRA-2=-0.039, ΔAODCAMSRA=-0.053).

2. In the case of speciated AODs, the differences in mean values from MERRA-2 and CAMSRA are greater than for total AOD. The highest absolute difference was found for organic aerosol (AOD_OCMERRA-2 $= 0.021 \pm 0.001$ and AOD_OMCAMSRA $= 0.055 \pm 0.002$) and sulphate aerosol (AOD_SUMERRA-2 $= 0.069 \pm 0.002$, AOD_SUCAMSRA=0.033 ± 0.001). The largest relative difference between reanalyses was found for dust, 185% of the mean AOD_DU value from the two reanalyses. The highest agreement between the reanalyses was obtained for sea salt aerosol (AOD_SSMERRA-2 $= 0.019 \pm 0.0003$, AOD_SSCAMSRA $= 0.018 \pm 0.0005$).

3. A south-to-north decreasing spatial distribution pattern is observed for all the speciated AODs, except for sea salt and organic carbon. Sea salt AOD decreases from the Skagerrak-Kattegat towards the Gulf of Bothnia and the Gulf of Finland. For organic carbon, CAMSRA yields a typical S-to-N AOD decrease, but in MERRA-2, an east-to-west gradient is observed in the period 1980–1999, and a nearly uniform distribution in 2003–2023.

4. During the period 1980–1999, the annual mean AOD averaged over the entire Baltic Sea decreased at a rate of 0.07 [−0.11; −0.05] per decade (ss90). During the period 2003–2023, the trends are much weaker, −0.006[−0.009; −0.002] 1/10y (−4.2%/10y) and statistically insignificant for MERRA-2 and −0.016[−0.021; −0.009] 1/10y (−11.6%/10y) and statistically significant (ss90) for CAMSRA. The trend values increase from south to north. The trends are stronger and statistically significant for the southern sectors with the largest magnitudes in the decades 2003–2023 in sector 6 for MERRA-2 (−0.009 [−0.012; −0.006] 1/10y; −5.8%/10y, s95) and for CAMSRA (−0.021 [−0.032; −0.014] 1/10y; −15.1%/10y; ns).

5. For the monthly mean AOD, significant seasonal variations in the trend values are observed, with a minimum in spring and a maximum in summer. In the years 2003–2023, the amplitude of the seasonal cycle of the trend of the monthly mean AOD averaged for the entire Baltic Sea was 0.04 1/10y for MERRA-2 and 0.03 1/10y for CAMSRA.

6. For the annual mean speciated AODs averaged over the entire Baltic Sea, trends differ between reanalyses. The largest difference is observed for AOD_OC/OM; the trend over 2003–2023 was positive for MERRA-2 0.005 [0.003; 0.006] 1/10y; s95) and negative for CAMSRA (−0.007 [−0.009; −0.006] 1/10y; ss95). The greatest agreement is found for AOD_SU −0.008 [−010; −0.005] 1/10y (ss95) and 0.009 [-0.015; -0.002] 1/10y (ss90), respectively), and AOD_SS (0.0009 [0.0001; 0.0016] 1/10y, ns; 0.002 [0.001; 0.003] 1/10y, ss95).

7. For AOD_OC/OM, AOD_SU, and AOD_BC from both reanalyses, as well as for AOD_DU from MERRA-2, significant seasonal variations in trend values are

observed, typically with minimum trend values in spring and maximum values in summer. The AOD_SU trend from CAMSRA also shows low values in summer. Despite a similar pattern of seasonal variability, the actual values may differ between reanalyses.

8. In the period 1980–1999, a single-peak AOD seasonal cycle was observed, with the highest values of AOD in spring. In 2003–2023, both reanalyses show a decrease in the spring peak and an increase in the summer peak. In the decade 2013–2023, the summer peak became dominant over both the northern and southern Baltic Sea. The dominance of the summer peak was also observed for AOD_BC, and AOD_OC/OM.

9. CAMSRA exhibits stronger seasonal variations in AOD, AOD_SU, AOD_BC and AOD_OC/OM than MERRA-2. Comparison of AOD measured at the AERONET Helsinki station with two reanalyses implies that the shape of the AERONET seasonal cycle is closer to the shape of the MERRA-2 seasonal cycle. However, MERRA-2 consistently overestimates the monthly mean AOD.

10. Spatial coherence of variability in total and speciated AOD in the northern and southern Baltic agrees between reanalyses. For the detrended annual means, the correlation coefficients are high and largely comparable: 0.79–0.87 for MERRA-2 and 0.60–0.89 for CAMSRA.

11. For sea-salt, black carbon and dust aerosol, magnitudes of AOD fluctuations (relative to respective trend line) are lower in the northern part of the Baltic than in the southern in both reanalyses. The ratios of the magnitudes are 0.64–0.96. AOD_OC (AOD_OM) shows very similar magnitude of fluctuations in southern and northern parts of the Baltic Sea (ratios of 0.97 and 1.07), while total AOD and AOD_SU from MERRA-2 and CAMSRA show different patterns – a decrease from south to north for AOD and AOD_SU from CAMSRA (0.90 and 0.59) and a weak increase or similar magnitude of fluctuations for AOD and AOD_SU from MERRA-2 (1.14 and 1.07).

12. For both reanalyses, the highest correlations between the monthly fire count and AOD and speciated AOD occur in April. The correlation coefficient between fire count and the monthly mean AOD averaged for the entire Baltic Sea is 0.67 and 0.68 for MERRA-2 and CAMSRA, respectively. The corresponding coefficients for AOD_BC are 0.83 and 0.71, and for AOD_SU, 0.68 and 0.66. The coefficients are statistically significant at the 0.01 level. In the case of AOD_OC/AOD_OM, a statistically significant correlation occurs only in CAMSRA (0.71).

13. A statistically significant correlation between total and speciated AODs and the NAO index was found mainly for the winter months. For both reanalyses, the highest correlation was observed at that time between the NAO index and AOD_SS, with correlation coefficients decreasing from December (0.77 for the entire Baltic Sea for MERRA-2 and 0.81 for CAMSRA) to February (0.51 for MERRA-2 and 0.54 for CAMSRA).

14. The reanalyses differ in the sign of the correlation coefficient between total AOD and the NAO index for the winter months. Statistically significant coefficients are positive for CAMSRA and negative for MERRA-2.

15. In July, CAMSRA AOD_SS correlates negatively with NAO (significant), which is consistent with summer NAO dynamics that modulate wind/storminess and hence marine aerosol production.

Total AOD patterns are broadly consistent between the reanalyses, whereas species-resolved AODs differ markedly. These differences are evident not only in their spatial distribution but also in their temporal behaviour, including trends, seasonal cycles, and interannual variability across regions and aerosol species. The reanalyses differ substantially in several aspects, including aerosol type representation, parameterisation of aerosol processes, emission inventories, data assimilation techniques, and underlying meteorological models. The comparative analysis presented in this study is based primarily on total and speciated AOD datasets, which limits the ability to fully identify the underlying causes of the observed differences.

The AOD differences between the reanalyses highlight the importance of exercising caution when using speciated AODs from reanalysis in source attribution or radiative closure studies. They also emphasise the need for systematic evaluation against independent observations – both column-integrated and in situ – to constrain model uncertainties related to temporal and spatial aerosol variability.

Acknowledgements

This work was carried out within the framework of IO PAS's statutory research (Polish Ministry of Science and Higher Education). This research was also supported by the National Science Centre grant SMART (grant no. 2023/49/B/ST10/00513).

The authors would like to thank the NASA Global Modeling and Assimilation Office (GMAO) and the team of the NASA GES-DISC Interactive Online Visualisation and Analysis Infrastructure (GIOVANNI) for providing MERRA-2 AOD data, Copernicus Atmosphere Monitoring Service and the CAMS Atmosphere Data Store for providing CAMSRA AOD data, the NOAA Climate Prediction Center for providing NAO indices, the NASA Fire Information for Resource

Management System (FIRMS), part of NASA's Earth Science Data and Information System (ESDIS) for providing fire information. The authors also thank Antti Arola, the principal investigator of the Helsinki AERONET site, and Veijo Aaltonen, the site manager, for access to the AERONET data used in this publication.

Authorship contribution statement

A. Rozwadowska: conceptualisation, resources, methodology, software, data processing, formal analysis, funding acquisition, writing – original draft. P. Markuszewski: writing – review and editing, funding acquisition.

Data availability

All the data supporting the findings of this paper can be accessed via the following links:
MERRA-2 AOD: https://giovanni.gsfc.nasa.gov/giovanni/ (Accessed on 10-09-2024), CAMSRA AOD: https://ads.atmosphere.copernicus.eu/datasets/cams-global-reanalysis-eac4-monthly?tab=download (Accessed on 20.10.2024), fire information: https://www.earthdata.nasa.gov/data/tools/firms (Accessed on 10-09-2024), NAO index: https://www.cpc.ncep.noaa.gov/products/precip/CWlink/pna/norm.nao.monthly.b5001.current.ascii.table (Accessed on 5.11.2024), AERONET AOD: https://aeronet.gsfc.nasa.gov/cgi-bin/data_display_aod_v3?site=Helsinki&nachal=2&level=2&place_code=10 (Accessed on 16.11.2024),

Supplementary material

Supplementary material associated with this article can be found here.

Conflict of interest

None declared.

References

Amarillo, A.C., Curci, G., De Santis, D., et al., 2024. *Validation of aerosol chemical composition and optical properties provided by Copernicus Atmosphere Monitoring Service (CAMS) using ground-based global data*. Atmos. Environ. 334, 120683. https://doi.org/10.1016/j.atmosenv.2024.120683

Ansmann, A., Bösenberg, J., Chaikovsky, A., et al., 2003. *Long-range transport of Saharan dust to northern Europe: The 11–16 October 2001 outbreak observed with EARLINET*. J. Geophys. Res. 108(D24), 4783. https://doi.org/10.1029/2003JD003757

Barnston, A.G., Livezey, R.E., 1987. *Classification, seasonality and persistence of low-frequency atmospheric circulation patterns*. Mon. Weather Rev. 115, 6, 1083–1126. https://doi.org/10.1175/1520-0493(1987)115<1083:CSAPOL>2.0.CO;2

Bladé, I., Liebmann, B., Fortuny, D., van Oldenborgh, G.J., 2012. *Observed and simulated impacts of the summer NAO in Europe: implications for projected drying in the Mediterranean region*. Clim. Dynam. 39, 709–727. https://doi.org/10.1007/s00382-011-1195-x

Bressi, M., Cavalli, F., Putaud, J.P., et al., 2021. *A European aerosol phenomenology – 7: High-time resolution chemical characteristics of submicron particulate matter across Europe*. Atmos. Environ.: X, 10, 100108, (Appendix). https://doi.org/10.1016/j.aeaoa.2021.100108

CAMS, 2020a. *CAMS global reanalysis (EAC4) monthly averaged fields*. Copernicus Atmosphere Monitoring Service (CAMS) Atmosphere Data Store, (Accessed on 20.10.2024). https://doi.org/10.24381/fd75fff2

CAMS, 2020b. *CAMS global reanalysis (EAC4) subdaily fields*. Copernicus Atmosphere Monitoring Service (CAMS) Atmosphere Data Store, (Appendix), (Accessed on 20.10.2024). https://doi.org/10.24381/d58bbf47

Chin, M., Ginoux, P., Kinne, S., et al., 2002. *Tropospheric aerosol optical thickness from the GOCART model and comparisons with satellite and sun photometer measurements*. J. Atmos. Sci. 59, 461–483. https://doi.org/10.1175/1520-0469(2002)059<0461:TAOTFT>2.0.CO;2

Christoudias, T., Pozzer, A., Lelieveld, J., 2012. *Influence of the North Atlantic Oscillation on air pollution transport*. Atmos. Chem. Phys. 12, 869–877. https://doi.org/10.5194/acp-12-869-2012

Colarco, P., da Silva, A., Chin, M., Diehl, T., 2010. *Online simulations of global aerosol distributions in the NASA GEOS-4 model and comparisons to satellite and ground-based aerosol optical depth*. J. Geophys. Res. 115, D14207. https://doi.org/10.1029/2009JD012820

Collaud Coen, M., Andrews, E., Bigi, A., Romanens, G., Martucci, G., Vuilleumier, L., 2020. *Effects of the prewhitening method, the time granularity and the time segmentation on the Mann–Kendall trend detection and the associated Sen's slope*, Atmos. Meas. Tech. 13, 6945–6964. https://doi.org/10.5194/amt-13-6945-2020

Darmenov, A.S., da Silva, A., 2015. *The Quick Fire Emissions Dataset (QFED): Documentation of Versions 2.1, 2.2 and 2.4*. Tech. Rep. Ser. Global Modeling and Data Assimilation, Vol. 38, Koster, R.D. (ed.) Goddard Space Flight Center, NASA, Greenbelt, MD, 201 pp., (Appendix). https://gmao.gsfc.nasa.gov/pubs/docs/Darmenov796.pdf

de Meij, A., Pozzer, A., Lelieveld, J., 2012. *Trend analysis in aerosol optical depths and pollutant emission estimates between 2000 and 2009*. Atmos. Environ. 51, 75–85. https://doi.org/10.1016/j.atmosenv.2012.01.059

Di Antonio, L., Di Biagio, C., Foret, G., et al., 2023. *Aerosol optical depth climatology from the high-resolution MAIAC product over Europe: differences between major European cities and their surrounding environments*. Atmos. Chem. Phys. 23, 12455–12475. https://doi.org/10.5194/acp-23-12455-2023

Diehl, T., Heil, A., Chin, M., et al., 2012. *Anthropogenic, biomass burning, and volcanic emissions of black carbon, organic carbon, and SO2 from 1980 to 2010 for hindcast model experiments*. Atmos. Chem. Phys. Discus. 12 (9), 24895–24954, (Appendix). https://doi.org/10.5194/acpd-12-24895-2012

Dong, B., Sutton, R.T., Woollings, T., Hodges, K., 2013. *Variability of the North Atlantic summer storm track: mechanisms and impacts on European climate*. Environ. Res. Lett. 8, 034037. https://doi.org/10.1088/1748-9326/8/3/034037

Duncan, B.N., Martin, R.V., Staudt, A.C., et al., 2003. *Interannual and seasonal variability of biomass burning emissions constrained by satellite observations*. J. Geophys. Res. 108 (D2), 4100, (Appendix). https://doi.org/10.1029/2002JD002378

Eck, T.F., Holben, B.N., Reid, J.S., et al., 1999. *Wavelength dependence of the optical depth of biomass burning, urban, and desert dust aerosols*, J. Geophys. Res. 104 (D24), 31333–31350, (Appendix).

European Commission, 2010. European Commission/Joint Research Centre (JRC)/Netherlands Environmental Assessment agency (PBL): Emission Database for Global Atmospheric Research (EDGAR), release ver. 4.1, (Appendix). https://edgar.jrc.ec.europa.eu

European Comission, 2011. European Commission/Joint Research Centre (JRC)/Netherlands Environmental Assessment agency (PBL): Emission Database for Global Atmospheric Research (EDGAR), release ver. 4.2, (Appendix). https://edgar.jrc.ec.europa.eu

Filonchyk, M., Hurynovich, V., Yan, H., Zhou, L., Gusev, A., 2020. *Climatology of aerosol optical depth over Eastern Europe based on 19 years (2000–2018) MODIS TERRA data*. Int. J. Climatol. 40, 3531–3549. https://doi.org/10.1002/joc.6412

Folland, C.K., Knight, J., Linderholm, H.W., et al., 2009. *The summer North Atlantic Oscillation: past, present, and future*. J. Clim. 22, 1082–103. https://doi.org/10.1175/2008JCLI2459.1

Friman, M., Aurela, A., Saarnio, K., et al., 2023. *Long-term characterization of organic and elemental carbon at three different background areas in northern Europe*. Atmos. Environ. 310, 119953. https://doi.org/10.1016/j.atmosenv.2023.119953

Giles, D.M., Sinyuk, A., Sorokin, M.G., et al., 2019. *Advancements in the Aerosol Robotic Network (AERONET) Version 3 database – automated near-real-time quality control algorithm with improved cloud screening for Sun photometer aerosol optical depth (AOD) measurements*, Atmos. Meas. Tech. 12, 169–209, (Appendix). https://doi.org/10.5194/amt-12-169-2019

Ginoux, P., Chin, M., Tegen, I., et al., 2001. *Sources and distributions of dust aerosols simulated with the GOCART model*. J. Geophys. Res. 106 (D17), 20255–20273, (Appendix). https://doi.org/10.1029/2000JD000053

Glantz, P., Fawole, O.G., Ström, J., et al., 2022. *Unmasking the effects of aerosols on greenhouse warming over Europe*. J. Geophys. Res.: Atmospheres 127, e2021JD035889. https://doi.org/10.1029/2021JD035889

Glantz, P., Freud, E., Johansson, C., et al., 2019. *Trends in MODIS and AERONET derived aerosol optical thickness over Northern Europe*. Tellus B 71(1), 1554414. https://doi.org/10.1080/16000889.2018.1554414

GMAO, 2015a. *MERRA-2 tavgM_2d_aer_Nx: 2d,Monthly mean,Time-averaged,Single-Level,Assimilation,Aerosol Diagnostics V5.12.4*, Greenbelt, MD, USA, Goddard Earth Sciences Data and Information Services Center (GES DISC), (Accessed on 10-09-2024). http://dx.doi.org/10.5067/FH9A0MLJPC7N

GMAO, 2015b. *MERRA-2 tavg1_2d_aer_Nx: 2d,1-Hourly, Time-averaged,Single-Level,Assimilation,AerosolDiagnostics V5.12.4*, Greenbelt, MD, USA, Goddard Earth Sciences Data and Information Services Center (GES DISC), (Appendix; Accessed on 10.09.2024). https://doi.org/10.5067/KLICLTZ8EM9D

GMAO, 2015c. *MERRA-2 tavgM_2d_slv_Nx: 2d,Monthly mean, Time-Averaged,Single-Level,Assimilation,Single-Level Diagnostics V5.12.4*, Greenbelt, MD, USA, Goddard Earth Sciences Data and Information Services Center (GES DISC), (Accessed on 8.03.2024). https://doi.org/10.5067/AP1B0BA5PD2K

Gong, S.L., 2003. *A arameterization of sea-salt aerosol source function for sub- and supermicron particles*. Global Biogeochem. Cy. 17(4), 1097, (Appendix). https://doi.org/10.1029/2003GB002079

Granier, C., Bessagnet, B., Bond, T., et al., 2011. *Evolution of anthropogenic and biomass burning emissions of air pollutants at global and regional scales during the 1980–2010 period*. Climate Change 109, 163–190. https://doi.org/10.1007/s10584-011-0154-1

Guenther, A., Hewitt, C.N., Erickson, D., et al., 1995. *A global model of natural volatile organic compound emissions*. J. Geophys. Res. 100 (D5), 8873–8892, (Appendix). https://doi.org/10.1029/94JD02950

Gueymard, C.A., Yang D., 2020. *Worldwide validation of CAMS and MERRA-2 reanalysis aerosol optical depth products using 15 years of AERONET observations*. Atmos. Environ. 225, 117216. https://doi.org/10.1016/j.atmosenv.2019.117216

Han, K.M., Jung, C.H., Song, C.H., et al., 2025. *Trends and classification of aerosol observed from MODIS sensor over Northern Europe and the Arctic*. Atmos. Pollut. Res. 16, 102329. https://doi.org/10.1016/j.apr.2024.102329

Holben, B.N., Eck, T.F., Slutsker, I., et al., 1998. *AERONET – a federated instrument network and data archive for aerosol characterization*. Remote Sens. Environ. 66 (1), 1–16, (Appendix). https://doi.org/10.1016/S0034-4257(98)00031-5

Inness, A., Ades, M., Agustí-Panareda, A., et al., 2019. *The CAMS reanalysis of atmospheric composition*. Atmos. Chem. Phys. 19, 3515–3556. https://doi.org/10.5194/acp-19-3515-2019

Kaiser, J.W., Heil, A., Andreae, M.O., et al., 2012. *Biomass burning emissions estimated with a global fire assimilation system based on observed fire radiative power*. Biogeosciences 9, 527–554, (Appendix). https://doi.org/10.5194/bg-9-527-2012

Karl, M., Jonson, J.E., Uppstu, A., et al., 2019. *Effects of ship emissions on air quality in the Baltic Sea region simulated with three different chemistry transport models*. Atmos. Chem. Phys. 19, 7019–7053. https://doi.org/10.5194/acp-19-7019-2019

Kecorius, S., Kivekäs, N., Kristensson, A., et al., 2016. *Significant increase of aerosol number concentrations in air masses crossing a densely trafficked sea area*. Oceanologia 58 (1), 1–12. https://doi.org/10.1016/j.oceano.2015.08.001

Lana, A., Bell, T.G., Simó, R., et al., 2011. *An updated climatology of surface dimethlysulfide concentrations and emission fluxes in the global ocean*. Global Biogeochem. Cy. 25 (1), GB1004, (Appendix). https://doi.org/10.1029/2010GB003850

Lehmann, A., Getzlaff, K., Harlaß, J., 2011. *Detailed assessment of climate variability in the Baltic Sea area for the period 1958 to 2009*. Clim Res. 46, 185–196. https://doi.org/10.3354/cr00876

Lewandowska, A.U., Śliwinska-Wilczewska, S., Woźniczka, D., 2017. *Identification of cyanobacteria and microalgae in aerosols of various sizes in the air over the Southern Baltic Sea*. Mar. Pollut. Bull. 125 (1–2), 30–38. https://doi.org/10.1016/j.marpolbul.2017.07.064

Lynch, P., Reid, J.S., Westphal, D.L., et al., 2016. *An 11-year global gridded aerosol optical thickness reanalysis (v1.0) for atmospheric and climate sciences*. Geosci. Model Dev. 9, 1489–1522. https://doi.org/10.5194/gmd-9-1489-2016

Maciszewska, A.E., Markowicz, K.M., Witek, M.L., 2010. *Multiyear analysis of aerosol optical thickness over Europe and Central Poland using NAAPS model simulation*. Acta Geophys. 58 (6), 1147–1163. https://doi.org/10.2478/s11600-010-0034-5

Mancinelli, E., Passerini, G., Virgili, S., Rizza, U., 2024. *Multi-decadal trends in aerosol optical depth of the main aerosol species based on MERRA-2 reanalysis: A case study in the Baltic Sea Basin*. Remote Sens. 16, 2421. https://doi.org/10.3390/rs16132421

Markowicz, K.M., Chilinski, M.T., Lisok, J., et al., 2016. *Study of aerosol optical properties during long-range transport of biomass burning from Canada to central Europe in July 2013*. J. Aerosol Sci. 101, 156–173. https://doi.org/10.1016/j.jaerosci.2016.08.006

Markowicz, K. M., Okrasa, I., Chilinski, M.T., et al., 2024. *Long term variability of the MERRA 2 radiation budget over Poland in Central Europe*. Acta Geophys. 72, 2907–2924. https://doi.org/10.1007/s11600-023-01256-5

Markowicz, K.M., Zawadzka-Manko, O., Posyniak, M., 2022. *A large reduction of direct aerosol cooling over Poland in the last decades*. Int. J. Climatol. 42(7), 4129–4146. https://doi.org/10.1002/joc.7488

Markuszewski, P, Kosecki, S, Petelski, T., 2017. *Sea spray aerosol fluxes in the Baltic Sea region: Comparison of the WAM model with measurements*. Estuar. Coast. Shelf Sci. 195, 16–22. https://doi.org/10.1016/j.ecss.2016.10.007

McCarty, J.L., Krylov, A.M., Prishchepov, A., et al., 2016. *Agricultural fires in European Russia, Belarus, and Lithuania and their impact on air quality, 2002–2012*. [in:] Gutman, G., Radeloff, V. (eds), *Land-Cover and Land-Use Changes in Eastern Europe after the Collapse of the Soviet Union in 1991*, Springer Nature, 247 pp. https://doi.org/10.1007/978-3-319-42638-9

Meier, H.E.M., Barghorn, L., Börgel, F., et al., 2023. *Multi-decadal climate variability dominated past trends in the water balance of the Baltic Sea watershed*. npj Clim. Atmos. Sci. 6, 58. https://doi.org/10.1038/s41612-023-00380-9

Meier M.H.E., Kniebusch, M., Dieterich, C., et al., 2022. *Climate change in the Baltic Sea region: a summary*. Earth Syst. Dynam. 13, 457–593. https://doi.org/10.5194/esd-13-457-2022

Monahan, E.C., Spiel, D.E., Davidson, K.L., 1986. *A model of marine aerosol generation via whitecaps and wave disruption*. [In:] Monahan, E.C., Niocaill, G.M. (eds.), *Oceanic Whitecaps and Their Role in Air-Sea Exchange Processes*. Springer, Dordrecht, 167–174, (Appendix). https://doi.org/10.1007/978-94-009-4668-2_16

Morcrette, J.-J., Boucher, O., Jones, L., et al., 2009. *Aerosol analysis and forecast in the European Centre for Medium-Range Weather Forecasts Integrated Forecast System: Forward modeling*. J. Geophys. Res. 114, D06206. https://doi.org/10.1029/2008JD011235

O'Neill, N.T., Eck, T.F., Holben, B.N., et al., 2001. *Bimodal size distribution influence on the variation of Angstrom derivatives in spectral and optical depth space*. J. Geo-

phys. Res. 106 (D9), 9787–9806, (Appendix). https://doi.org/10.1029/2000JD900245

Petelski, T., Markuszewski, P., Makuch, P., et al., 2014. *Studies of vertical coarse aerosol fluxes in the boundary layer over the Baltic Sea*. Oceanologia 56(4), 697–710. https://doi.org/10.5697/oc.56-4.697

Randerson, J.T., Liu, H., Flanner, M.G., et al., 2006. *The impact of boreal forest fire on climate warming*. Science 314 (5802), 1130–1132, (Appendix). https://doi.org/10.1126/science.1132075

Randles, C.A., da Silva, A.M., Buchard, V., et al., 2017. *The MERRA-2 aerosol reanalysis, 1980 onward. Part I: System description and data assimilation evaluation*. J. Climate 30, 6823–6850. https://doi.org/10.1175/JCLI-D-16-0609.1

Rozwadowska, A., Kratzer, S., 2016. *The impact of air mass advection on aerosol optical properties over Gotland (Baltic Sea)*. Atmos. Res. 182, 142–155. https://doi.org/10.1016/j.atmosres.2016.07.022

Rutgersson, A., Jaagus, J., Schenk, F., Stendel, M., 2014. *Observed changes and variability of atmospheric parameters in the Baltic Sea region during the last 200 years*. Clim Res. 61, 177–190. https://doi.org/10.3354/cr01244

Shang, X., Mielonen, T., Lipponen, A., et al., 2021. *Mass concentration estimates of long-range-transported Canadian biomass burning aerosols from a multi-wavelength Raman polarization lidar and a ceilometer in Finland*. Atmos. Meas. Tech. 14, 6159–6179. https://doi.org/10.5194/amt-14-6159-2021

Sindelarova, K., Granier, C., Bouarar, I., et al., 2014. *Global data set of biogenic VOC emissions calculated by the MEGAN model over the last 30 years*. Atmos. Chem. Phys. 14, 9317–9341, (Appendix). https://doi.org/10.5194/acp-14-9317-2014

Sinyuk, A., Holben, B.N., Eck, T.F., et al., 2020. *The AERONET Version 3 aerosol retrieval algorithm, associated uncertainties and comparisons to Version 2*. Atmos. Meas. Tech. 13, 3375–3411, (Appendix). https://doi.org/10.5194/amt-13-3375-2020

Stein, O., Schultz, M.G., Bouarar, I., et al., 2014. *On the wintertime low bias of Northern Hemisphere carbon monoxide found in global model simulations*. Atmos. Chem. Phys. 14, 9295–9316, (Appendix). https://doi.org/10.5194/acp-14-9295-2014

Thakur, R.C., Dada, L., Beck, L.J., et al., 2022. *An evaluation of new particle formation events in Helsinki during a Baltic Sea cyanobacterial summer bloom*. Atmos. Chem. Phys. 22 (9), 6365–6391. https://doi.org/10.5194/acp-22-6365-2022

Witthuhn, J., Hünerbein, A., Filipitsch, F., 2021. *Aerosol properties and aerosol–radiation interactions in clear-sky conditions over Germany*. Atmos. Chem. Phys. 21, 14591–14630. https://doi.org/10.5194/acp-21-14591-2021

Xian, P., Reid, J.R., Ades, M., et al., 2024. *Intercomparison of aerosol optical depths from four reanalyses and their multi-reanalysis consensus*. Atmos. Chem. Phys. 24, 6385–6411. https://doi.org/10.5194/acp-24-6385-2024

Yang, Y., Lou, S., Wang, H., et al., 2020. *Trends and source apportionment of aerosols in Europe during 1980–2018*. Atmos. Chem. Phys. 20, 2579–2590. https://doi.org/10.5194/acp-20-2579-2020

Yumimoto, K., Tanaka, T.Y., Oshima, N., Maki, T., 2024. *JRAero: the Japanese Reanalysis for Aerosol v1.0.* Geosci. Model Dev. 10, 3225–3253. https://doi.org/10.5194/gmd-10-3225-2017

Zdun, A., Rozwadowska, A., Kratzer, S., 2011. *Seasonal variability in the optical properties of Baltic aerosols*. Oceanologia 53(1), 7–34. https://doi.org/10.5697/oc.53-1.007